NASA Contractor Report 194930

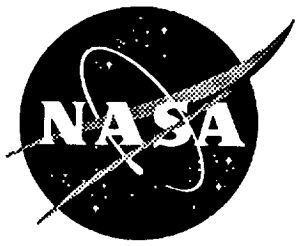

Analysis of Woven and Braided Fabric Reinforced Composites

Rajiv A. Naik
Analytical Services & Materials, Inc., Hampton, Virginia

Contract NAS1-19399
June 1994

National Aeronautics and
Space Administration
Langley Research Center
Hampton, Virginia 23681-0001

ANALYSIS OF WOVEN AND BRAIDED FABRIC REINFORCED COMPOSITES

Rajiv A. Naik
Analytical Services & Materials, Inc.

ABSTRACT

A general purpose micromechanics analysis that discretely models the yarn architecture within the textile repeating unit cell, was developed to predict overall, three dimensional, thermal and mechanical properties. This analytical technique was implemented in a user-friendly, personal computer-based, windows compatible code called Textile Composite Analysis for Design (TEXCAD). TEXCAD was used to analyze plain, 5-harness satin, and 8-harness satin weave composites along with 2-D braided and 2x2, 2-D triaxial braided composites. The calculated overall stiffnesses correlated well with available 3-D finite element results and test data for both the woven and the braided composites. Parametric studies were performed to investigate the effects of yarn size on the yarn crimp and the overall thermal and mechanical constants for plain weave composites. The effects of braid angle were investigated for the 2-D braided composites. Finally, the effects of fiber volume fraction on the yarn undulations and the thermal and mechanical properties of 2x2, 2-D triaxial braided composites were also investigated.

Key Words: textile composites, modeling, plain weave, satin weave, triaxial braid, yarn, crimp, design, thermal, stiffness, elastic properties.

INTRODUCTION

Composite materials reinforced with woven and braided fabric preforms are being considered for potential structural applications in the aircraft and automotive industries. Fabric-reinforced 'textile' composites potentially have better out-of-plane stiffness, strength, and, toughness properties than tape laminates. They are also amenable to automated and efficient manufacturing techniques. However, the architecture of a textile composite is complex and, therefore, the parameters controlling its mechanical properties are numerous. This necessitates development of analytical models to predict the thermal and mechanical properties of textile composites. The present study focuses on the analysis of woven and braided textile composites.

Fabric Architecture

A two-dimensional (2-D) woven composite laminate is one of the simplest textile composites and it consists of stacked, pre-impregnated layers of woven fabric [1] which are cured and consolidated by a process similar to tape laminates. The fabric is composed of two sets of interlacing, mutually orthogonal (warp and fill) yarns (Fig. 1). Each yarn is a bundle of filaments (or fibers) and the yarn size is measured by the number of filaments in the yarn. The fabric is woven on a loom and its architecture is characterized by the interlacing pattern of the warp and fill yarns. Some of the commonly used weave architectures are the plain weave, 5-harness satin and 8-harness satin weaves (see Fig. 1). The periodicity of the repeating pattern in a woven (or braided) fabric can be used to isolate a small repeating unit cell (RUC) which is sufficient to describe the fabric architecture. The RUC for the plain, 5- and 8-harness satin weaves are indicated in Fig. 1 by dark borders. The interlacing of the yarns in a fabric leads to yarn undulation or 'crimp'. Composite stiffness properties are governed by (i) weave parameters such as weave architecture, yarn sizes, yarn spacing, and yarn crimp; (ii) laminate parameters such as stacking orientations and overall fiber volume fraction; and (iii) material parameters such as yarn and resin stiffnesses.

Braided preforms are fabricated over a cylindrical mandrel. A single layer of a 2-D braid consists of either two or three intertwined yarns. The braider yarns follow the $+\theta$ and $-\theta$ directions and usually interlace in either a 1 x 1 or a 2 x 2 pattern (see Fig. 2). A 1 x 1 pattern is similar to the interlacing in a plain weave fabric (see Fig. 2(a)). In a 2 x 2 pattern a $+\theta$ braider yarn continuously passes over two $-\theta$ braider yarns and then under two $-\theta$ braider yarns and vice versa. A 2-D triaxial braid consists of axial yarns in addition to the off-axis braider yarns (see Fig. 2(b)). The axial yarns follow the longitudinal direction and are inserted between the braider yarns.

A 2-D braided composite laminate of a certain desired thickness is formed by overbraiding layers of the desired architecture on top of each other. After the preform is removed from the mandrel, slit along the axial direction, flattened and border stitched, resin is introduced by a resin transfer molding process. This leads to a two dimensional material as there are no interlayer yarns through the laminate thickness. Composite stiffness properties are governed by (i) braid parameters such as braid architecture, yarn sizes, yarn spacing, and yarn crimp; and (ii) material parameters such as yarn and resin stiffnesses and overall fiber volume fraction.

Typical photomicrographs for a 2x2, 2-D braided laminate are shown in Fig. 3. The longitudinal section (Fig. 3(a)) along the axial yarns indicates minor crimp in these yarns. Fig. 3(b) shows a transverse section of the laminate. The lenticular cross-sectional shape of the axial yarns is evident. Also, the axial yarns do not stack on top of one another. This is due to nesting between layers during the brading operation. Fig. 3(c) shows a section along the braider yarns. The degree of crimp in the braider yarns as they intertwine is well illustrated in this section.

Analytical Techniques

A number of analytical and numerical techniques have been used to analyze both woven and braided composites. All of the proposed models exploit the periodicity of the textile

architecture to isolate a representative unit cell (RUC). The RUC is assumed to lie in the interior of the composite away from edge effects. Overall properties are calculated by making certain assumptions about the RUC internal geometry and deformation field. A review of the analytical models used in the past was presented by Raju, Foye, and Avva [2]. Some of the earlier models for analyzing woven and braided composites are highlighted below.

Chou and Ishikawa [3] presented three different models for 2-D woven composites based on classical lamination theory (CLT) - the mosaic model, the fiber undulation model, and the bridging model. The mosaic model neglected the undulation of the yarns and idealized the RUC as an assemblage of asymmetric cross-ply laminates. The fiber undulation model considered the undulation in the fill yarn direction but neglected the undulation in the warp yarns. The bridging model extended the applicability of the fiber undulation model to the analysis of satin weave composites (Fig. 1) by separately modeling the straight portions of the yarns.

The fabric geometry model (FGM) [4] was another model based on CLT. It combined textile engineering methodology and a modified laminate theory. The geometric model consisted of straight yarns oriented in six different directions. Such a unit cell representation neglected the crimp in the yarns. The FGM was also used together with an energy analysis [5] to predict stiffness properties of three-dimensional (3-D) braided composites. The FGM model was further modified by Pastore and Gowayed [6]. The fiber inclination model (FIM) [7] was also based on CLT. It treated the fabric unit cell as an assemblage of inclined unidirectional laminae. The FIM also neglected the crimp in the yarns. Ramnath [8] presented an approach that used a variable yarn cross-section geometry model along with admissible displacement and stress fileds to determine bounds on the elastic properties of 2-D woven composites.

Naik and Ganesh [9] and Raju and Wang [10] developed models for woven composites that accounted for undulations in both the fill and the warp yarns. They computed overall stiffness properties by assuming either iso-strain or iso-stress or a combination of these and analytically integrating through the volume of the RUC. Due to the tedious analytical

description of yarn cross-sectional shapes and yarn paths and the analytical volume integrations, this approach is not well suited for the analysis of more complicated architectures such as 2-D braids and 2-D triaxial braids.

Three-dimensional (3-D) finite element models (FEM) [11-15] have also been developed for the analysis of plain weave composites. The 3-D FEM are highly computer intensive and also require considerable time and effort for model generation. Foye [13] developed inhomogeneous finite elements and analyzed sub-cells within the RUC to overcome these limitations. He analyzed many textile architectures including plain and satin weaves, 2-D braids, and 2-D triaxial braids. However, he had to manually calculate the stiffness properties, after estimating the material directions and volume fractions, for each element in the 3-D model. FEM is, therefore, not well suited for performing parametric studies to investigate the sensitivity of overall mechanical properties to architecture parameters.

Naik, Masters and Ifju [16] presented a simple but accurate geometric modeling and analysis technique for 2-D triaxially braided composites. They discretely modeled the yarn centerline paths within the RUC by assuming sinusoidal undulations and used a yarn discretization scheme together with a 3-D stress averaging procedure to compute overall stiffness properties which correlated well with test data over a wide range of architecture parameters. The objective of the present study was to extend this modeling approach to the development of a general purpose analysis technique that could (i) discretely model the internal yarn architecture and (ii) calculate overall thermal and mechanical properties for a variety of woven and braided composite materials, such as, plain and satin weaves (Fig. 1), 2-D braids and 2-D triaxial braids (Fig. 2) and other textile architectures. Another objective of this effort was to develop a technique that was accurate enough to provide good estimates of overall properties over a wide range of architecture parameters while being simple enough to be performed on a personal computer.

ANALYTICAL PROCEDURES

The analysis of a fabric reinforced composite requires, first, a proper three dimensional description of the preform architecture. The geometric modeling of the preform architecture was performed, in the present study, by utilizing the periodicity of the textile composite to isolate a repeating unit cell (RUC). For each yarn within the RUC the yarn centerline path was then described by assuming a flattened lenticular cross-sectional shape for the interlacing yarns. This assumption was based on the lenticular yarn cross-sectional shapes observed in micrographs of the composite (see Fig. 3). Details of the geometric modeling technique and its applications to various woven and braided architectures are included in the following sections. Having described the fiber architecture, the three dimensional effective stiffnesses for the composite were computed by first discretizing each yarn in the RUC into yarn slices and then using the material properties, spatial orientation, and volume fraction of each yarn slice in a volume averaging technique that assumed an iso-strain state within the RUC.

Geometric Modeling of Plain Weave Composites

The RUC for the 2-D plain weave composite is shown in Fig. 4. The sectional view in Fig. 4 (section A-A) shows the undulations of a warp yarn as it crosses over and under the fill yarns. Only one layer of the plain weave is shown in the sectional view. The analysis of stacked woven and braided layers is discussed in a following section.

The plain weave composite is usually specified by known quantities such as yarn spacing, a, in the fill and warp directions, yarn filament count, n, for the fill and warp yarns, yarn packing density, p_d, filament diameter, d_f, and overall fiber volume fraction, V_f. These known quantities were used to determine the unknown quantities such as yarn thicknesses, yarn cross-sectional areas, yarn crimp angle and yarn undulating paths which are required to discretely model each yarn within the RUC. For the sake of simplicity, the yarn spacings and yarn fiber counts for the fill and warp directions were assumed to be equal in the following derivation.

The yarn cross-sectional area, A, was assumed to be the same for both the warp and fill yarns and also to remain constant along the entire yarn path. The projected length, L_p, of the yarn path for each yarn was a function of the yarn spacing, a, and was given by $L_p = 2\,a$ (see Fig. 4). The volume occupied by the four yarns within the RUC was given by $4\,A\,L_p$. The dimensions of the RUC were $L_p \times L_p \times H$, where H was the RUC thickness. The volume of the RUC not occupied by the yarns was assigned to the interstitial matrix. For a yarn packing density of p_d, the overall fiber volume fraction, V_f, for the RUC in Fig. 4 can be derived as:

$$V_f = \frac{2\,p_d\,A}{H\,a} \tag{1}$$

Using the yarn filament count, n, and filament diameter, d_f, the unknown cross-sectional area, A, for the yarns was calculated as:

$$A = \frac{\pi\,d_f^2\,n}{4\,p_d} \tag{2}$$

For a given overall fiber volume fraction, the unknown thickness, H, was calculated using Eqns. (1) and (2). The quantity p_d may either be determined by image analysis of photomicrographs of sections through the thickness of the composite or may be assumed to be between 0.7 - 0.8. The yarn thickness, t, was related to the RUC thickness, H, by $t = H/2$. The yarn width, w, was calculated by assuming complete coverage (i.e. no gap between adjacent yarns) and was given by $w = a$.

The yarn path for each of the four yarns in the RUC consists of two straight portions and three undulating portions. The undulations are centered around cross-over points (COP) where a yarn crosses over or under another yarn (see Fig. 4). In each of the three undulating portions, the yarns were assumed to follow a sinusoidal path. The sine function used to

describe the yarn centerline path had its origin at the COP and was determined by the vertical shift, V_s, and the undulating length, L_u. For a warp yarn, for example, the undulation, Z_c, at each COP was expressed as:

$$Z_c = \pm \frac{V_s}{2} \sin\left(\frac{\pi X_c}{L_u}\right) \tag{3}$$

where, X_c was measured from the corresponding COP along the warp yarn direction. A negative sign was used in Eqn.(3) to describe the undulation, at the central COP, for the warp yarn shown in section A-A (see Fig. 4). A positive sign was used in Eqn. (3) to describe the undulations at the COPs located on the RUC edges for the same warp yarn. Only half the sine wave was used to describe the yarn centerline paths at the edge COPs. The centerline path for the other warp yarn in the RUC was described in a similar manner by using Eqn. (3) with the appropriate sign and sine wave portion at each COP. The undulations in the fill yarns were also described by Eqn. (3) by measuring X_c along the fill yarn direction (*i.e.* along the Y-axis).

For the plain weave architecture, the vertical shift, V_s, in Eqn. (3) was equal to the thickness, t, of the yarns. The parameter, L_u, was determined by considering the cross-sectional shape of the yarns which consisted of a central flat portion of thickness, t, and two sinusoidal lenticular end portions as shown in Fig. 4. The curved portions of the yarn cross-section were assumed to be described by the sinusoidal functional form of Eqn. (3). Thus, the width of the curved portion of the yarn cross-section was equal to $L_u/2$. The cross-sectional area, A, was expressed as:

$$A = w\,t - L_u\,V_s\left(1 - \frac{2}{\pi}\right) \tag{4}$$

The unknown parameter, L_u, was calculated using Eqns. (2) and (4). The total length of the straight portions, L_{st}, of each yarn was expressed as:

$$L_{st} = 2\,a - 2\,L_u \tag{5}$$

Thus, Eqns. (1) - (5) were used to determine all the required geometry parameters for the plain weave RUC, which included, the yarn cross-sectional area, yarn thickness, and, yarn paths based on a knowlegde of the yarn filament counts, yarn spacing, yarn packing density, filament diameter, and overall fiber volume fraction. Note that, Eqn. (4) is valid for $w \geq L_u$ which physically implies that the parameter, L_u, (also the total width of the curved portions of the yarn cross-section) cannot exceed the spacing, a, between the yarns.

The undulation in the yarns is often described by its "crimp angle". In the present study, the crimp angle (see Fig. 4) was defined as the positive angle between the tangent to the sinusoidal yarn centerline path and the X-Y plane (see Fig. 4) at a COP. Thus, the crimp angle, θ_c, was expressed as:

$$\tan(\theta_c) = \left| \left(\frac{dZ_c}{dX_c} \right)_{X_c=0} \right| \tag{6}$$

In general, $\theta_{min} \leq \theta_c \leq (\pi/2)$, where, θ_{min}, was the minimum θ_c for a given plain weave architecture and was determined by the constraint $w \geq L_u$.

Geometric Modeling of Satin Weave Composites

The RUCs for the 5-harness satin weave and the 8-harness satin weave are shown in Figs. 5 and 6, respectively. The sectional views in Figs. 5 and 6 (section A-A) show the undulations of a warp yarn as it crosses over and under the fill yarns.

The architecture modeling for the satin weave composite was similar to the plain weave composite. The yarn cross-sectional area, A, was assumed to be the same and to remain constant for each yarn in the RUC. The projected length, L_p, of the yarn path for each yarn and, A, were used to calculate the volume occupied by the yarns within the RUC. The volume occupied by the yarns within the RUC was given by $2\ h\ A\ L_p$ where $h = 5$ for a 5-harness satin weave and $h = 8$ for a 8-harness satin weave. The projected length, L_p, was a function of the yarn spacing, a, and was given by $L_p = h\ a$ (see Figs. 5 and 6). The dimensions of the RUC were $L_p \times L_p \times H$, where H was the RUC thickness. The volume of the RUC not occupied by the yarns was assigned to the interstitial matrix in the RUC. The yarn width, w, was related to the yarn spacing, a, by assuming complete coverage and was given by $w = a$. For a yarn packing density of p_d, the overall fiber volume fraction, V_f, for the 5- and 8-harness satin weave architectures can be shown to be given by Eqn. (1). The yarn cross-sectional area, A, for both the satin weave architectures was calculated using Eqn. (2). The RUC thickness, H, was then calculated using Eqns. (1) and (2) for both satin weaves. Yarn thickness, t, was given by $t = (H/2)$.

The yarn undulations were centered around either two or three cross-over points for the satin weaves. For example, for the 5-harness satin weave, the warp yarns in the first, third, and fourth rows from the top (Fig. 5) had two COPs, while warp yarns in the second and fifth (section A-A) rows had three COPs. The sine function given by Eqn. (3) was used to describe the yarn centerline paths at the COPs with the appropriate sign and sine wave portion at each COP.

For both the satin weave architectures, the vertical shift, V_s, in Eqn. (3) was equal to the thickness, t, of the yarns. The parameter, L_u, which was also the total width of the curved portion of the cross-sectional shape of the yarns (see Fig. 4) was calculated using Eqns. (2) and (4). The total length of the straight portion of each yarn was given by:

$$L_{st} = h\ a - 2\ L_u \qquad (7)$$

where h = 5 for 5-harness satin weaves and h = 8 for 8-harness satin weaves. Thus, Eqns. (1) - (4), (7) were used to determine the geometry of the 5- and 8-harness satin weave composites. The crimp angle, θ_c, was given by Eqn. (6) and the constraint $w \geq L_u$ was used to determine θ_{min}. Note that, Eqn. (7) can be substituted for Eqn. (5) by using h = 2 for the plain weave composite, thereby, generalizing the formulation for the plain, 5-harness satin, and, 8-harness satin weave composites.

Geometric Modeling of 2-D Braided Composites

The RUC for the 2-D braided architecture is shown in Fig. 7. The sectional view in Fig. 7 (section A-A) shows the undulations of a $+\theta$ braider yarn as it crosses over and under the $-\theta$ braider yarns. The architecture modeling for the 2-D braided composite was similar to the plain weave composite. However, unlike the plain weave, the braider yarns, in a 2-D braid, interlace at non-orthogonal angles. This fact was accounted for in determining the yarn paths in a 2-D braid. The yarn projected length, L_p, was a function of the yarn spacing, a, (perpendicular to the yarn direction) and the braid angle, θ_{br}, and was given by:

$$L_p = \frac{2\,a}{\sin(2\theta_{br})} \tag{8}$$

where θ_{br} was measured with respect to the Y-axis (see Fig. 7).

As in the plain weave, the yarn cross-sectional area, A, was assumed to be the same and to remain constant for each yarn in the RUC. The projected length, L_p, of the yarn path for each yarn and, A, were used to calculate the volume occupied by the yarns within the RUC. The volume occupied by the four yarns within the RUC was given by $4\,A\,L_p$. The dimensions of the parallelepiped RUC were $L_p \times L_p \times H$, where H was the RUC thickness and included angle between the two sides with length, L_p, was $2\theta_{br}$. The volume of the RUC not

occupied by the yarns was assigned to the interstitial matrix in the RUC. The yarn width, w, (perpendicular to the yarn direction) was related to the yarn spacing, a, by assuming complete coverage and was given by $w = a$. For a yarn packing density of p_d, the overall fiber volume fraction, V_f, for the 2-D braid can be shown to be given by Eqn. (1). The yarn cross-sectional area, A, for the 2-D braided architecture was calculated using Eqn. (2). The RUC thickness, H, was then calculated using Eqns. (1) and (2). Yarn thickness, t, was given by $t = (H/2)$.

As in the plain weave architecture, the yarn undulations for the 2-D braid are centered around three cross-over points for each yarn. The sine function given by

$$Z_c = \pm \frac{V_s}{2} \sin\left(\frac{\pi X_c \sin(2\theta_{br})}{L_u}\right) \tag{9}$$

where, X_c is measured from the corresponding COP along the braider yarn direction, was used to describe the yarn centerline paths at the COPs with the appropriate sign and sine wave portion at each COP. The vertical shift, V_s, in Eqn. (9) was equal to the thickness, t, of the braider yarns. The cross-sectional shape of the braider yarns (perpendicular to the braider yarn direction) was similar to that shown in Fig. 4 and consisted of a central flat portion of thickness, t, and two sinusoidal lenticular end portions of width, $L_u/2$. The total width, L_u, was calculated using Eqns. (2) and (4). The total length of the straight portion of each yarn path, L_{st}, (along the braider yarn direction) was given by

$$L_{st} = \frac{2\,(a - L_u)}{\sin(2\theta_{br})} \tag{10}$$

Thus, Eqns. (1), (2), (4), (9) and (10) were used to determine the geometry of the 2-D braided composites. The crimp angle, θ_c, was determined by using Eqns. (6) and (9) and the limitation $w \geq L_u$ was used to determine θ_{min}.

Geometric Modeling of 2-D Triaxial Braided Composites

The RUC used for the 2x2, 2-D triaxial braid is shown in Fig. 8. The sectional view A-A shows the undulation of a braider yarn which undulates over and under the axial yarns in the RUC. The 2-D triaxial braided composite is usually specified by known quantities such as braid angle, θ_{br}, axial yarn spacing, d_o, yarn filament counts for the axial and braider yarns, n_o and n_b, respectively, yarn packing density, p_d, filament diameter, d_f, and overall fiber volume fraction, V_f. These known quantities were used to determine the unknown quantities such as yarn thicknesses, yarn cross-sectional areas, yarn crimp angle and yarn undulating paths which are required to discretely model each yarn within the RUC. A detailed description of the geometric modeling approach for the 2x2, 2-D triaxial braided composite was presented in Ref. 16. Simplified equations for the same geometric model are presented here.

As before, the yarn cross-sectional areas, A_o, and A_b, for the axial and braider yarns, respectively, were assumed to remain constant along the entire yarn path. The projected lengths, L_o and L_b, of the axial and braider yarn paths were a function of the axial yarn spacing, d_o, and the braid angle, θ_{br}, and were given by $L_o = 8\, d_o \cot(\theta_{br})$ and $L_b = 2\, d_o/\sin(\theta_{br})$, respectively. Note that L_o represents the total projected length of the four axial yarns within the RUC. The total volume occupied by the axial and braider yarns was given by $(A_o L_o + 8 L_b A_b)$. The dimensions of the parallelepiped RUC were $L_b \times L_b \times H$, where H was the RUC thickness and the included angle between the two sides with length, L_b, was $2\theta_{br}$. The volume of the RUC not occupied by the yarns was assigned to the interstitial matrix in the RUC. For a yarn packing density of p_d, the overall fiber volume fraction, V_f, for the RUC in Fig. 8 was derived as:

$$V_f = \frac{p_d \, (A_o \sin(2\theta_{br}) + 4 \, A_b \sin(\theta_{br}))}{H \, d_o \sin(2\theta_{br})} \tag{11}$$

where, H is the thickness of the RUC. Using the known yarn filament counts, n_o and n_b, filament diameter, d_f, the unknown cross-sectional areas, A_o and A_b, for the axial and braider yarns, respectively, were calculated using Eqn. (2). For a given overall fiber volume fraction, the unknown thickness, H, was then calculated using Eqn. (11). The braider yarn thickness, t_b, was a function of the RUC thickness, H, and the yarn thickness ratio, m

$$t_b = \frac{H}{2 + m}, \qquad m = \frac{t_o}{t_b} \tag{12}$$

where t_o was the thickness of the axial yarns. The unknown yarn thickness ratio, m, was determined recursively as described below. The braider yarn width, w_b, (perpendicular to the yarn direction) was calculated by assuming complete coverage (i.e. no gap between adjacent yarns) and was given by

$$w_b = d_o \cos(\theta_{br}) \tag{13}$$

The yarn path for the axial yarns was assumed to be straight throughout the RUC. The braider yarn path consisted of straight portions and undulating portions. In the undulating portion the braider yarn was assumed to follow a sinusoidal path at each COP. The sine function used to describe the braider yarn centerline path, Z_c, at each COP was expressed as:

$$Z_c = \pm \frac{V_a}{2} \sin\left(\frac{\pi \, X_c \sin(\theta_{br})}{L_u}\right) \tag{14}$$

where, X_c was measured from the corresponding COP along the braider yarn direction. Eqn. (14) was used to describe the yarn centerline paths at the COPs with the appropriate sign and sine wave portion at each COP. The vertical shift, V_s, in Eqn. (14) was equal to the sum of the axial and braider yarn thicknesses and was given by $V_s = t_o + t_b$.

The parameter, L_u, was determined by considering the cross-sectional areas, A_o and A_b, of the axial and braider yarns which were expressed by Eqns. (15) and (16), respectively, as:

$$A_o = w_o t_o - L_u V_s \left(1 - \frac{2}{\pi}(s + \cos(s))\right), \qquad s = \sin^{-1}\left(\frac{1}{1+m}\right) \tag{15}$$

where, $w_o = d_o - 2\,s\,(L_u/\pi)$ was the width of the axial yarns, and

$$A_b = w_b t_b - \frac{2}{\pi} L_u \left(t_b s - V_s (1 - \cos(s))\right) \tag{16}$$

The unknown parameters, L_u and m, were determined by a recursive solution of Eqns. (15) and (16) in which A_o and A_b were calculated using Eqn. (2). The total length of the straight portion of each braider yarn was given by

$$L_{st} = \frac{2\,(d_o - L_u)}{\sin(\theta_{br})} \tag{17}$$

Thus, Eqns. (2), (11) - (17) were used to determine the geometry of the 2x2, 2-D, triaxial braided composites. The crimp angle, θ_c, was given by Eqns. (6) and (14) and the limitations $w_b \geq L_u\,(2\,s/\pi)$ and $w_o \geq L_u\,(1 - (2\,s/\pi))$ were used to determine the θ_{min}.

Discretization of Yarns

Overall composite properties were determined by discretizing each of the yarns within the RUC. The straight portions of each yarn path were modeled as a single slice with length, L_{st}. Along an undulating portion, the yarn was divided into n, equal, piecewise straight slices made perpendicular to its in-plane direction and normal to the X-Y plane (Fig. 8). Thus, the undulating, sinusoidal yarn path was approximated by n interconnected straight yarn slices. The volume of each yarn slice was computed as $(A_y L_y/n)$ where A_y and L_y are the yarn cross-sectional area and the length of the undulating portion, respectively. Note that, $L_y = L_u$ for the woven architectures (Figs. 4-6) and $L_y = L_u'$ for the braided architectures (Figs. 7, 8).

The spatial orientation of each yarn slice was described by the in-plane angle, θ, that it made with the X-axis (Fig. 8) and the out-of-plane angle, β, that it made with the X-Y plane. For the woven architectures, the angle θ was either 0 (warp yarns) or 90 (fill yarns) degrees. For the braided composites, the angle θ, for the braider yarns, was determined from a knowledge of the braid angle. The angle β, for both woven and braided architectures, was calculated, for each yarn slice, by differentiating the sine function used to describe the undulating yarn centerline path. For the yarn slice that modeled the straight portions of the yarn path, $\beta = 0$ was used.

Thus, each yarn in the RUC was approximated by straight yarn slices with known volumes and known orientation angles θ and β. The total volume occupied by all the yarn slices was subtracted from the volume of the RUC to compute the volume occupied by the interstitial matrix pockets in the RUC. The interstitial matrix was represented as an isotropic material slice having orientation angles $\theta = \beta = 0$.

Calculation of Three-Dimensional Effective Stiffnesses

For the purpose of calculating overall properties, the RUC of the textile composite was treated as a spatially oriented fiber composite composed of yarn slices with transversely

isotropic material properties and longitudinal material axes oriented at known angles θ and β. A stress averaging technique [17] based on an iso-strain assumption within the RUC was used to compute overall composite properties as described below.

The three-dimensional thermoelastic stress-strain relations, in global XYZ coordinates, for the composite RUC were defined using effective material properties to relate the average values of the state variables. Using the usual contracted notation [18], the stress-strain relation was written in matrix form as

$$\{\bar{\sigma}\} = [C_{eff}] \left(\{\bar{\varepsilon}\} - \{\bar{\alpha}\}\, \Delta T\right) \tag{18}$$

where $\{\bar{\sigma}\} = \{\overline{\sigma_{xx}}, \overline{\sigma_{yy}}, \overline{\sigma_{zz}}, \overline{\sigma_{xy}}, \overline{\sigma_{yz}}, \overline{\sigma_{zx}}\}$, the overbar denotes average values over the RUC, $\{\bar{\varepsilon}\} = \{\overline{\varepsilon_{xx}}, \overline{\varepsilon_{yy}}, \overline{\varepsilon_{zz}}, \overline{\varepsilon_{xy}}, \overline{\varepsilon_{yz}}, \overline{\varepsilon_{zx}}\}$, $\{\bar{\alpha}\} = \{\overline{\alpha_{xx}}, \overline{\alpha_{yy}}, \overline{\alpha_{zz}}, 0, 0, 0\}$ are the overall coefficients of thermal expansion (CTE), ΔT is the change in temperature and $[C_{eff}]$ is a 6x6 matrix [18] of the overall, three-dimensional effective stiffnesses of the composite.

For a set of displacement boundary conditions applied to the RUC the average strains in the composite were given by $\{\bar{\varepsilon}\}$. The following procedure was used to determine $\{\bar{\sigma}\}$. An iso-strain state was assumed to exist within the RUC. This provided for compatibility among yarn slices and also led to displacements that satisfied the boundary conditions. In the global RUC coordinates (XYZ coordinates), the strains in each yarn slice were, therefore, given by

$$\{\varepsilon\}_m = \{\bar{\varepsilon}\} \tag{19}$$

where the subscript m denotes the m^{th} yarn slice. Knowing the strains and assuming an isothermal state in the RUC, yarn slice stresses in the local yarn slice material coordinate system (123 coordinates) (see Fig. 8) were computed as

$$\{\sigma'\}_m = [C']_m \left(\{\varepsilon'\}_m - \{\alpha'\}_m \Delta T\right)$$

where, (20)

$$\{\varepsilon'\}_m = [T]_m \{\varepsilon\}_m$$

The 6x6 stiffness matrix $[C']_m$ defines the three-dimensional stress-strain relationship for the m^{th} yarn slice which is assumed to be a transversely isotropic material and $\{\alpha'\}_m$ are the CTE for the m^{th} yarn slice. The five independent material constants (E_{11}, E_{22}, G_{12}, ν_{12}, and ν_{23}, subscript 1 corresponds to the axial fiber direction) that are required to define the $[C']_m$ matrix and the yarn slice CTE α_{11}, α_{22} and α_{33} could be measured quantities based on yarn tests. They could also be estimated by a rule of mixtures or a micromechanics analysis from constituent properties. Such an estimate would require a knowledge of fiber properties, matrix properties and the yarn packing density p_d (or yarn fiber volume fraction). The transformation matrix $[T]_m$ for the strains in Eq. (20) is defined in Appendix A.

The average stresses in the RUC were found by first transforming yarn slice stresses to the global RUC coordinates and then computing the volume average of the stresses in all the yarn slices as

$$\{\bar{\sigma}\} = \sum_{m=1}^{N} V_m \{\sigma\}_m$$

where, (21)

$$\{\sigma\}_m = [T]_m^T \{\sigma'\}_m$$

where V_m is the volume fraction of the m^{th} yarn slice in the RUC and N is the total number of yarn slices (including the interstitial matrix material slice) in the RUC. The $[T]_m^T$ matrix is the transpose of the matrix $[T]_m$ defined in Eqn. (A1) and is used to transform stresses from yarn slice material coordinates (123) to the global RUC coordinates (XYZ).

Based on Eqns. (18) - (21) the effective stiffness matrix $[C_{eff}]$ of the RUC was written in terms of the yarn slice stiffness matrices, transformation matrices and volume fractions as

$$[C_{eff}] = \sum_{m=1}^{N}\left(V_m[T]_m^T\left[C'\right]_m[T]_m\right) \tag{22}$$

and the overall CTEs for the RUC were given by

$$[\bar{\alpha}] = \left[C_{eff}\right]^{-1}\left\{\sum_{m=1}^{N}\left(V_m[T]_m^T\left[C'\right]_m\left\{\alpha'\right\}_m\right)\right\} \tag{23}$$

A convergence study was performed to determine the appropriate number of yarn slices, n, in the undulating portions of the yarns, required to yield converged values for the overall stiffnesses $[C_{eff}]$. The computed stiffnesses for the woven and braided composites in the present study were found to be unchanged for $n \geq 12$. A value of $n = 12$ was used for all the analyses in this study. The overall stiffness matrix $[C_{eff}]$ was inverted to obtain the overall compliance matrix $[S_{eff}]$ which was used to determine overall moduli and Poisson's ratios [18].

Analysis of Stacked Oriented Textile Layers

For laminates made by stacking layers with different orientations, the thermo-elastic properties for each layer can be obtained from the models described in the preceeding sections,

using appropriate tensor transformations. For the layered textile composite laminate, it is assumed that classical lamination theory can be used to compute thermal and mechanical laminate properties. Each layer of the textile is treated as a lamina in this analysis. Nesting between the layers, by which layers slide into the available space in the adjacent layers, is not accounted for in the present framework of the classical lamination scheme.

RESULTS AND DISCUSSION

The above geometric modeling and analytical technique, for textile composite overall thermo-mechanical properties, was implemented in a user-friendly, windows compatible, personal computer-based code called Textile Composite Analysis for Design (TEXCAD). TEXCAD is also capable of predicting textile composite damage onset, damage growth, failure modes and ultimate strength. The formulation for the strength analysis will be presented in a subsequent paper. In the present paper, TEXCAD was used to analyze 2-D woven (plain, 5- and 8-harness satin), 2-D braided, and 2x2, 2-D triaxial braided composites. The calculated overall stiffnesses were correlated with available 3-D finite element (FEM) results and test data. Parametric studies were also performed to study the effects of various fabric parameters on overall properties.

All the analyses in the present study were made for yarns made of Hercules AS4 graphite fibers impregnated with Hercules 3501-6 epoxy matrix. A yarn fiber packing density, p_d, of 0.75 and a fiber diameter, d_f, of 0.007 mm was used in all calculations. The thermo-mechanical properties used for the impregnated yarns (V_f = 75%) and the resin are given in Table 1. The CTE's for the impregnated yarns with a 75% fiber content were calculated using a micromechanics analysis based on an Airy's stress function approach for a square fiber packing [21]. The CTE for the 3501-6 epoxy resin ($40 \times 10^{-6}/^{o}C$) was available in the literature [22]. The CTE's for the fiber ($\alpha_{11} = -0.61 \times 10^{-6}/^{o}C$ and $\alpha_{22} = 3.8 \times 10^{-6}/^{o}C$) were back-calculated using the square array micromechanics model [21] together with the available

CTE's for the resin and for a unidirectional 60% fiber volume fraction AS4/3501-6 laminate. The laminate CTE's were taken from manufacturers data sheets [23].

Woven Composites

The thermal and mechanical elastic constants for plain, 5-harness satin and 8-harness satin weave composites calculated using TEXCAD (the present analysis) are shown in Table 2. The calculated results correlated well with finite element (FEM) results and test data reported in Ref. 13. A yarn spacing of 1.411 mm and an overall fiber volume fraction, V_f, of 64% [13] were used for all the three woven architectures. The yarn size was not specified in Ref. 13. It was, therefore, assumed to be 3 k (k - one thousand filaments) for both the fill and warp yarns. Using the geometric modeling approach described earlier, a 3 k yarn size led to a 19.4 degree crimp angle for the given yarn spacing and V_f. The crimp angle, for the plain weave composite, measured from the micrographs in Ref. 13, varied between 8 and 18 degrees. A 3 k yarn size was also used for calculating the results in Table 2 for the 5-harness satin and 8-harness satin weave composites.

Table 2 also includes results for a $[0/90/r]_s$ laminate (r - resin layer) calculated using classical lamination theory (CLT). To allow a direct comparison with the woven composites, the 0 and 90 degree plies were assigned the impregnated yarn (V_f = 75%) material properties (Table 1). Since the yarns (plies) had a 75% fiber content, a resin layer, r, was added to the cross-ply laminate to achieve an overall composite V_f = 64%. The volume fraction of the resin layer in the laminate was equal to that of the interstitial matrix in the woven composites. The CLT results further verify the trends in the results for the three architectures. Since the plain, 5-harness satin and 8-harness satin weaves have increasing amounts of yarn straight sections, L_{st}, (see Eqns. (5) and (7)) their moduli and CTE's should approach those of the cross-ply laminate.

Woven composite prepreg is often manufactured in different yarn sizes, such as, 3 k, 6 k, and 12 k. A parametric study was performed, using TEXCAD, to investigate the effects

of yarn size on the overall thermal and mechanical properties. Figure 9 shows the effects of yarn size on the crimp angle and the stiffness properties for a plain weave composite. For the same yarn spacing, yarn packing density and overall composite volume fraction, the crimp angle increased significantly with increasing yarn size. The in-plane moduli, E_{xx} and E_{yy}, decreased while, E_{zz}, increased with increasing yarn size. The shear moduli, the in-plane Poisson's ratio, ν_{xy}, (Fig. 9) and the in-plane CTE's, α_{xx} and α_{yy}, (see Fig. 10) were not very sensitive to yarn size effects. However, the through-thickness CTE, α_{zz}, (Fig. 10) and Poisson's ratios, ν_{xz} and ν_{yz}, (Fig. 9) were very sensitive to yarn size.

Note that, since the overall composite V_f and interstitial matrix volume fraction was kept constant while the yarn size was varied, a CLT-based analysis would have predicted no change in the overall properties with varying yarn size. It is, therefore, necessary to explicitly model the yarn architecture and crimp to investigate the effects of fabric parameters on overall thermal and mechanical properties of textile composites.

2-D Braided Composites

A yarn spacing of 1.411 mm (perpendicular to the yarn axial direction) and an overall fiber volume fraction, V_f, of 64% were used for the 2-D braided composites analyzed. As in the plain weave composite, a 2 k yarn size, a 0.75 yarn packing density, and a 0.007 mm fiber diameter were used for calculating the results for the different 2-D braided composites. A parametric study was performed to study the effects of braid angle variations on composite properties. Figures 11 and 12 show the effects of braid angle on the crimp angle, thermal, and mechanical properties of the 2-D braided composites. A good correlation was obtained with FEM results [13] for a 45 degree braid angle for the same braid parameters (Fig. 11). Since the 45 degree braided composite is equivalent to a plain weave composite rotated by 45 degrees (see Figs. 4 and 7), the computed results for a 45 degree braided composite were also verified by transforming the plain weave stiffnesses by 45 degrees.

The in-plane properties, E_{xx}, E_{yy}, G_{xy} and ν_{xy}, varied significantly with braid angle (Fig. 11). Through-thickness Poisson's ratios, ν_{xz} and ν_{yz}, and modulus, E_{zz}, were less sensitive to braid angle. Crimp angle (Fig. 12) varied between 6.7 and 13.2 degrees for braid angles between 15 and 75 degrees. The in-plane CTE's, α_{xx}, and α_{yy}, varied significantly with braid angle. Through-thickness CTE, α_{zz}, was less sensitive to braid angle.

2x2, 2-D Triaxial Braided Composites

The three different triaxial braided composites tested in Ref. 19 were analyzed using the present TEXCAD analysis. The yarn architecture parameters such as braid angle, braider and axial yarn sizes, axial yarn spacing and overall composite volume fraction for the three architectures (A1, B1, B2) are given in Table 3. These parameters along with a yarn packing density of 0.75 and a fiber diameter of 0.007 mm were used as input to TEXCAD for calculating the results in Table 4. The specimens in Ref. 19 were made with AS4 graphite fiber yarns and Shell 1895 epoxy resin. It was assumed that the 1895 epoxy had the same material properties as the 3501-6 resin (Table 1). Thus, the material properties for the impregnated yarns and the resin in Table 1 were used in the present analysis of 2-D triaxial braids.

Correlations of the computed elastic constants (Table 4) with test data [19] and FEM results [13, 19] were very good for all the three architectures. Further testing will be required to verify the results for the in-plane shear moduli, the through-thickness properties and the CTE's. It was shown in Ref. 16 that the results for in-plane moduli (including G_{xy}) and Poisson' ratio using the present analysis technique correlated well with test data over a wide range of architecture parameters for 2x2, 2-D triaxial braided composites. Parametric studies were also conducted in Ref. 16 to investigate the effects of braid angle, yarn size, and axial yarn content on overall stiffness properties of triaxial braided composites.

The overall fiber volume fraction for a textile composite, measured after fabrication, can often differ by a few percent from the specified fiber content. Furthermore, variations

may occur in the fiber volume fraction from one composite plate to another. It is, therefore, important to investigate the sensitivity of overall thermal and mechanical properties to fiber volume fraction. Figures 13 and 14 show results (for the B1 architecture) for the effects of fiber volume fraction on the thermal and mechanical properties of triaxial braided composites. Except for E_{xx} and E_{yy}, which increased proportionately with V_f, the shear moduli, E_{zz}, the Poisson's ratios and the in-plane CTE's (Fig. 14) were not very sensitive to variations in V_f. For a 9% increase in V_f (55% to 60%), E_{xx} and E_{yy} increased by about 8.3%. This trend in the E_{xx} was further verified by test data (see Fig. 13) for the B1 architecture [20]. Figure 14 shows that the crimp angle increased while the α_{zz} decreased significantly with increasing V_f.

SUMMARY

A general purpose micromechanics analysis that discretely models the yarn architecture within the textile repeating unit cell, was developed to predict overall, three dimensional, thermal and mechanical properties. This analytical technique was implemented in a user-friendly, personal computer-based, windows compatible code called Textile Composite Analysis for Design (TEXCAD). TEXCAD was used to analyze plain, 5-harness satin, and 8-harness satin weave composites along with 2-D braided and 2x2, 2-D triaxial braided composites. The calculated overall stiffnesses correlated well with available 3-D finite element results and test data.

Based on a parametric study performed on plain weave composites, it was found that for the same yarn spacing, yarn packing density and overall composite volume fraction, the crimp angle increased significantly with increasing yarn size. The in-plane moduli, E_{xx} and E_{yy}, decreased while, E_{zz}, increased with increasing yarn size. The shear moduli, the in-plane Poisson's ratio, ν_{xy}, and the in-plane CTE's, α_{xx} and α_{yy}, were not very sensitive to yarn size effects. However, the through-thickness CTE, α_{zz}, and Poisson's ratios, ν_{xz} and ν_{yz}, were very sensitive to yarn size.

The effects of braid angle were investigated for the 2-D braided composites. The in-plane properties, E_{xx}, E_{yy}, G_{xy} and ν_{xy}, varied significantly with braid angle. Through-thickness Poisson's ratios, ν_{xz} and ν_{yz}, and modulus, E_{zz}, were less sensitive to braid angle. Crimp angle varied between 6.7 and 13.2 degrees for braid angles between 15 and 75 degrees. The in-plane CTE's, α_{xx}, and α_{yy}, varied significantly with braid angle. Through-thickness CTE, α_{zz}, was less sensitive to braid angle.

The effects of fiber volume fraction on the thermal and mechanical properties of 2x2, 2-D triaxial braided composites were also investigated. Except for E_{xx} and E_{yy}, which increase proportionately with V_f, the shear moduli, E_{zz}, the Poisson's ratios and the in-plane CTE's were not very sensitive to variations in V_f. For a 9% increase in V_f (55% to 60%), E_{xx} and E_{yy} increased by about 8.3%. The crimp angle increased while the α_{zz} decreased significantly with increasing V_f.

The present TEXCAD analysis provides a useful tool for the prediction of thermo-elastic constants for a wide range of textile composite architectures. It also provides a means to conduct sensitivity studies for the numerous parameters that can affect the properties of textile composites. Finally, it has the potential for being implemented as an element constitutive model in a finite element formulation, thus, providing the capability of structural analysis for textile composite structures.

ACKNOWLEDGMENT

This work was supported by NASA under Contract Nos. NAS1-19399 and NAS1-19708. The author wishes to thank Dr. John E. Masters for providing the micrographs in Figure 3.

APPENDIX A

The transformation matrix $[T]_m$ for the strains in Eq. (20) is defined as [16]

$$[T]_m = \begin{bmatrix} a_{11}^2 & a_{12}^2 & a_{13}^2 & a_{12}a_{13} & a_{11}a_{13} & a_{11}a_{12} \\ a_{21}^2 & a_{22}^2 & a_{23}^2 & a_{22}a_{23} & a_{23}a_{21} & a_{21}a_{22} \\ a_{31}^2 & a_{32}^2 & a_{33}^2 & a_{32}a_{33} & a_{33}a_{31} & a_{31}a_{32} \\ 2a_{21}a_{31} & 2a_{32}a_{22} & 2a_{23}a_{33} & (a_{22}a_{33}+a_{23}a_{32}) & (a_{23}a_{31}+a_{21}a_{33}) & (a_{21}a_{32}+a_{22}a_{31}) \\ 2a_{11}a_{31} & 2a_{12}a_{32} & 2a_{13}a_{33} & (a_{32}a_{13}+a_{33}a_{12}) & (a_{11}a_{33}+a_{13}a_{31}) & (a_{31}a_{12}+a_{32}a_{11}) \\ 2a_{11}a_{21} & 2a_{12}a_{22} & 2a_{13}a_{23} & (a_{12}a_{23}+a_{13}a_{22}) & (a_{13}a_{21}+a_{11}a_{23}) & (a_{11}a_{22}+a_{12}a_{21}) \end{bmatrix} \tag{A1}$$

where a_{ij} (i = 1-3, j = 1-3) are the direction cosines between the yarn slice material coordinate axes (123) and the global RUC axes (XYZ) (see Fig. 8). For a yarn slice with its longitudinal material axis (1-axis) oriented at angles θ and β with respect to the global RUC coordinates, the 3x3, $[a_{ij}]$ matrix (i = 1-3, j = 1-3) is given by

$$[a_{ij}] = \begin{bmatrix} \cos(\theta)\cos(\beta) & \sin(\theta)\cos(\beta) & \sin(\beta) \\ -\sin(\theta) & \cos(\theta) & 0 \\ -\cos(\theta)\sin(\beta) & -\sin(\theta)\sin(\beta) & \cos(\beta) \end{bmatrix} \tag{A2}$$

Equation (A2) was derived by assuming that the 2-axis (i.e. the in-plane transverse direction, see Fig. 8) of the yarn slice was always perpendicular to the global Z-axis for any θ or β rotation of the yarn slice 1-axis (i.e. the axial fiber direction). This merely simplified the definition of the direction cosines without compromising the generality of the approach.

REFERENCES

1. Bailey, J. A.: "Woven Fabric Aerospace Structures," *Handbook of Composites, Vol. 2 - Structures and Design*, C. T. Herakovich and Y. M. Tarnopol'skii, Eds., 1989, pp. 354-391, Elsevier Science Publishers B. V.

2. Raju, I. S., Foye, R. L. and Avva, V. S.: "A Review of Analytical Methods for Fabric and Textile Composites," Proceedings of Indo-US Workshop on Composite Materials for Aerospace Applications, Bangalore, India, July 23-27, 1990, available as Composite Structures, Testing, Analysis and Design, J. N. Reddy and A. V. Krishna Murty, Eds., 1992, pp. 274-293, Narosa Publishing House, New Delhi, India.

3. Chou, T-W. and Ishikawa, T.: "Analysis and Modeling of Two-Dimensional Fabric Composites," *Composite Materials Series 3, Textile Structural Composites*, T-W. Chou and F. K. Ko, Eds., 1989, pp. 210-264, Elsevier Science Publishers B. V.

4. Ko, F. K., Pastore, C. M., Lei, C. and Whyte, D. W.: "A Fabric Geometry Model for 3-D Braid Reinforced FP/Al-Li Composites," International SAMPE Metals Conference: Competitive Advances in Metals/ Metal Processing, Cherry Hill, NJ, August 1987.

5. Ma, C-L., Yang, J-M and Chou, T-W.: "Elastic Stiffness of Three-Dimensional Braided Textile Structural Composites," *Composite Materials: Testing and Design (Seventh Conference), ASTM STP 893*, J. M. Whitney, Ed., American Society for Testing and Materials, Philadelphia, 1986, pp. 404-421.

6. Pastore, C. M. and Gowayed, Y. A.: "A Self-Consistent Fabric Geometry Model: Modification and Application of a Fabric Geometry Model to Predict the Elastic Properties of Textile Composites," *Journal of Composites Technology and Research*, JCTRER, Vol. 16, No. 1, Jan. 1994, pp. 32-36.

7. Yang, J-M., Ma, C-L. and Chou, T-W.: "Fiber Inclination Model of Three-Dimensional Textile Structural Composites," *Journal of Composite Materials*, Vol. 20, September 1986, pp. 472-484.

8. Ramnath, V.: "Elastic Properties of Woven Fabric Reinforced Composites," Proceedings of the 26th Structures, Structural Dynamics and Materials Conference, Orlando, Florida, April 15-17, American Institute of Aeronautics and Astronautics, 1985, Technical Papers, Part 1, A85-0720, pp. 420-425.

9. Naik, N. K. and Ganesh, V. K.: "Prediction of On-Axes Elastic Properties of Plain Weave Fabric Composites," *Composites Science and Technology*, Vol. 45, 1992, pp. 135-152.

10. Raju, I. S. and Wang, J. T.: "Classical Laminate Theory Models for Woven Fabric Composites," NASA TM 109087, February 1994, National Aeronautics and Space Administration, Hampton, Virginia.

11. Dasgupta, A., Bhandarkar, M., Pecht, M. and Barker, D.: "Thermo-Elastic Properties of Woven-Fabric Composites Using Homogenization Techniques," Proceedings of the American Society for Composites, Fifth Technical Conference, June 12-14, 1990, East Lansing, Michigan, 1990, pp. 1001-1010.

12. Whitcomb, J. D.: "Three-Dimensional Stress Analysis of Plain Weave Composites," *Composite Materials: Fatigue and Fracture (Third Volume), ASTM STP 1110*, T. K. O'Brien, Ed., American Society for Testing and Materials, 1991, pp. 417-438.

13. Foye, R. L.: "Finite Element Analysis of the Stiffness of Fabric Reinforced Composites," NASA CR-189597, Feb. 1992, National Aeronautics and Space Administration, Hampton, Virginia.

14. Raju, I. S., Craft, W. J. and Avva, V. S.: "Thermal Expansion Characteristics of Woven Fabric Composites," Proceedings of the International Conference on Structural Testing, Analysis, and Design, ICSTAD, Bangalore, India, July 29-August 3, 1990, pp. 3-10.

15. Blackketter, D. M., Walrath, D. E. and Hansen, A. C.: "Modeling Damage in a Plain Weave Fabric-Reinforced Composite Material," *Journal of Composites Technology and Research*, JCTRER, Vol. 15, No. 2, Summer 1993, pp. 136-142.

16. Naik, R. A., Ifju, P. G. and Masters, J. E.: "Effect of Fiber Architecture Parameters on Mechanical Performance of Braided Composites", Proceedings of the 4th NASA/ DOD Advanced Composites Technology Conference, Jun. 7-11, 1993, Salt Lake City, Utah, NASA CP 3229, Part 1, Vol. 1, pp. 525-554.

17. Rosen, B. W., Chatterjee, S. N. and Kibler, J. J.: "An Analysis Model for Spatially Oriented Fiber Composites," *Composite Materials: Testing and Design (Fourth Conference), ASTM STP 617*, American Society for Testing and Materials, 1977, pp. 243-254.

18. Jones, R. M., *Mechanics of Composite Materials*, Scripta Book Company, Washington, D. C., 1975.

19. Masters, J. E., Foye, R. L., Pastore, C. M. and Gowayed, Y. A.: "Mechanical Properties of Triaxially Braided Composites: Experimental and Analytical Results," *Journal of Composites Technology and Research*, JCTRER, Vol. 15, No. 2, Summer 1993, pp. 112-122.

20. Masters, J. E, Fedro, M. J. and Ifju, P. G.: "An Experimental and Analytical Characterization of Three Triaxially Braided Textile Composites," Proceedings of the Third NASA Advanced Composites Technology Conference, NASA CP 3178, Part 1, Vol. I, 1992, pp. 263-286.

21. Naik, R. A. and Crews, J. H., Jr.: "Micromechanical Analysis of Fiber-Matrix Interface Stresses Under Thermomechanical Loadings," *Composite Materials: Testing and Design (Eleventh Volume), ASTM STP 1206*, E. T. Camponeschi, Jr., Ed., American Society for Testing and Materials, 1993, pp. 205-219.

22. Adams, D. F. and Schaffer, B. G.: "Analytical/Experimental Correlations of Stiffness Properties of Unidirectional Composites," *Composites Technology Review*, Vol. 4, No. 2, Summer 1982, pp. 45-48.

23. "Hercules Prepreg Tape Materials Characterization Data Package; Fibers: AS4, IM6, IM7 & IM8; Resins: 8551-7, 8551-7A, 8552, 3501-6," Hercules, Inc., Magna, Utah, February 1989.

Table 1.- Yarn and resin properties used in the analysis [13, 16, 21, 22, 23].

Material	E_{11}, GPa	E_{22}, GPa	G_{12}, GPa	ν_{12}	ν_{23}	CTE α_{11}, 10^{-6}/°C	CTE α_{22}, 10^{-6}/°C
Yarn	144.80	11.73	5.52	0.23	0.30	-0.324	14.000
Resin	3.45	3.45	1.28	0.35	0.35	40.000	40.000

Note: The 1-axis is along the fiber direction, the 2-axis is perpendicular to the fibers but in the plane of the lamina and the 3-axis is in the out-of-plane direction.

Table 2.- Comparison of results for woven composites.

Laminate type	Approach	E_{xx}, E_{yy}, GPa	E_{zz}, GPA	G_{xz}, G_{yz}, GPa	G_{xy}, GPa	ν_{xz}, ν_{yz}	ν_{xy}	α_{xx}, α_{yy}, 10^{-6}/°C	α_{zz}, 10^{-6}/°C
Plain weave	TEXCAD	64.38	11.49	5.64	4.87	.396	.027	1.334	20.712
	FEM [13]	63.78	11.38	4.97	4.82	.329	.031	-	-
	Test [13]	61.92	-	-	-	-	.110	-	-
5-harness satin weave	TEXCAD	66.33	11.51	4.93	4.89	.342	.034	1.462	21.242
	FEM [13]	65.99	11.38	5.03	4.96	.320	.030	-	-
	Test [13]	69.43	-	-	5.24	-	.060	-	-
8-harness satin weave	TEXCAD	66.81	11.51	4.76	4.89	.329	.035	1.494	21.381
	FEM [13]	66.74	11.45	5.03	4.96	.320	.030	-	-
	Test [13]	72.19	-	-	6.76	-	.060	-	-
$[0/90/r^1]_s$ laminate	CLT	67.60	-	-	4.89	-	.038	1.548	-

[1]The r represents a resin layer used in the laminate to simulate the effect of the interstitial matrix in the woven composite.

Table 3.- Input parameters for 2x2, 2-D triaxial braided composites [19].

2-D triaxial braid	Braid angle, degrees	Braider yarn size, k	Axial yarn size, k	Axial yarn spacing, mm	Overall fiber volume fraction, %
A1	62.3	12	24	6.096	54.0
B1	67.4	6	18	5.320	51.2
B2	67.9	6	18	5.820	52.0

Table 4.- Comparison of results for 2x2, 2-D triaxial braided composites.

Braid type	Approach	E_{xx}, GPa	E_{yy}, GPA	E_{zz}, GPa	G_{xy}, GPa	G_{xz}, GPa	G_{yz}, GPa	ν_{xy}	α_{xx}, $10^{-6}/^{o}C$	α_{yy}, $10^{-6}/^{o}C$
A1	TEXCAD	45.14	40.10	10.42	14.84	4.64	4.13	.291	1.675	2.650
	FEM [19]	53.16	46.95	-	-	-	-	.305	-	-
	Test [19]	45.44	45.64	-	-	-	-	.307	-	-
B1	TEXCAD	48.42	42.48	10.13	11.07	4.40	3.90	.205	1.937	2.901
	FEM [19]	62.12	47.51	-	-	-	-	.211	-	-
	Test [19]	44.47	45.16	-	-	-	-	.199	-	-
B2	TEXCAD	50.42	42.63	10.23	11.08	4.31	3.90	.205	1.870	2.897
	FEM[1] [19]	51.09	43.58	12.07	12.41	-	-	.214	-	-
	Test [19]	48.47	43.51	-	-	-	-	.190	-	-

[1]The E_{zz} and G_{xy} were reported in Ref. [13] for the B2 architecture.

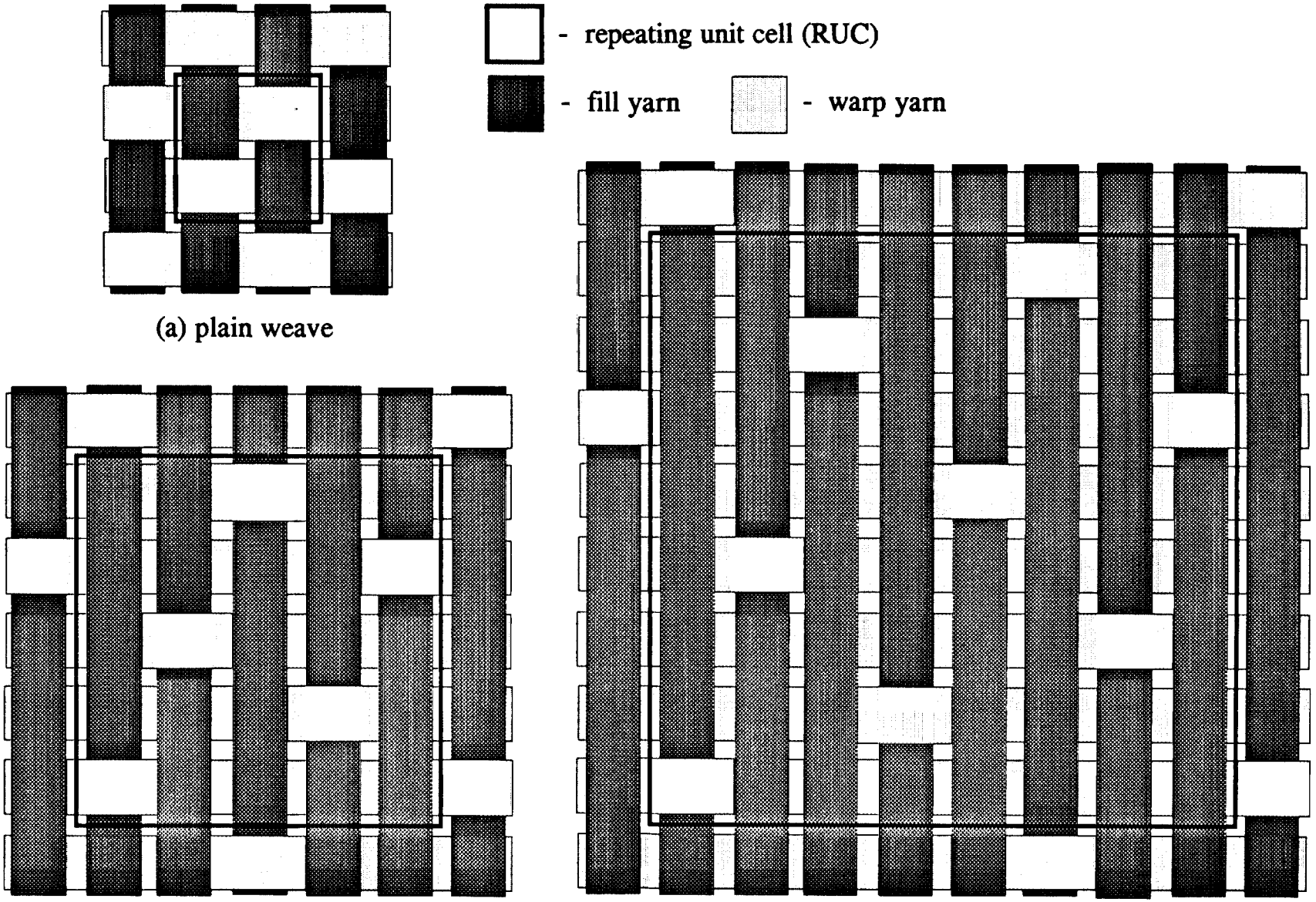

Fig. 1.- Typical yarn interlacing patterns for woven fabrics.

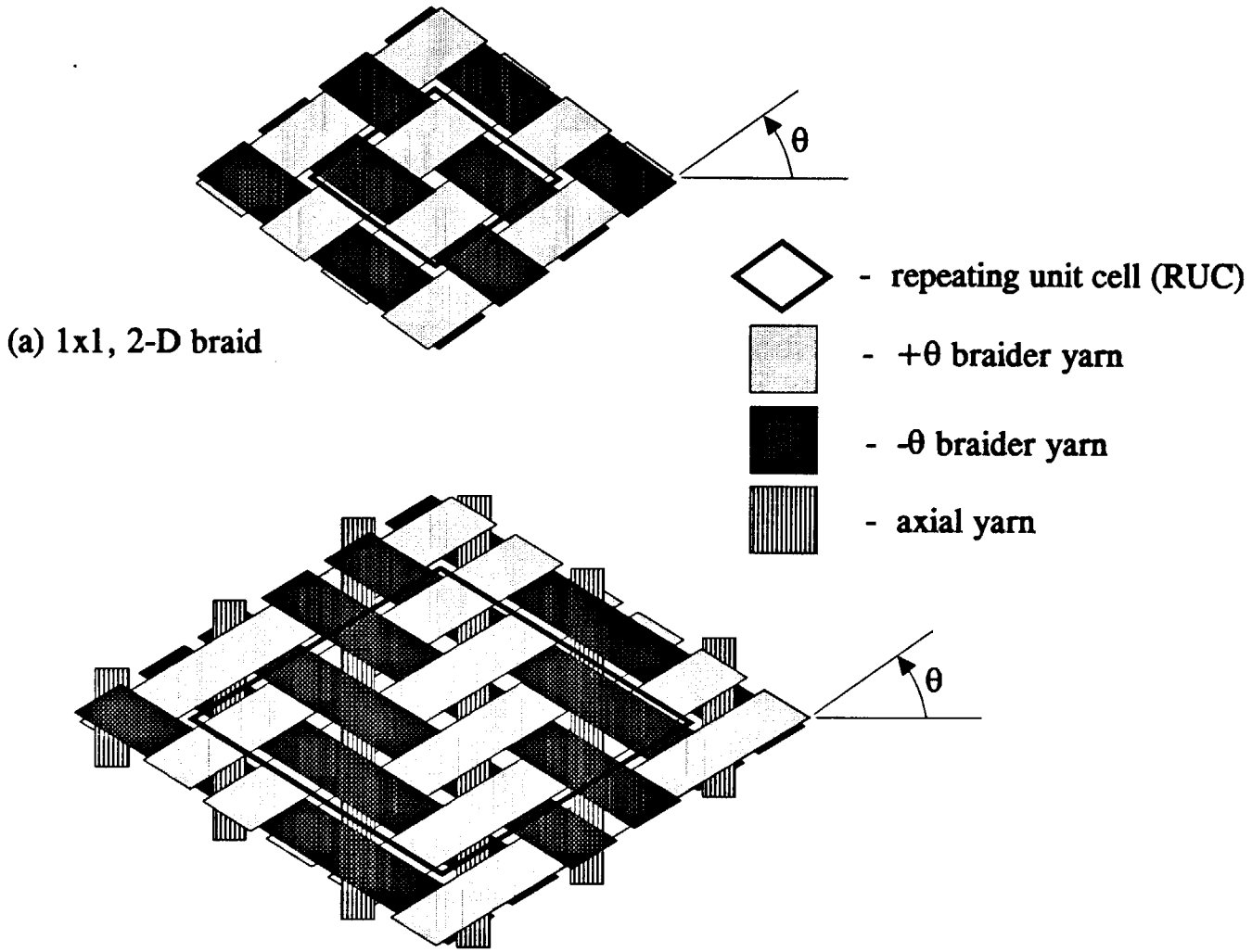

Fig. 2.- Typical yarn interlacing patterns for 2-D braided fabrics.

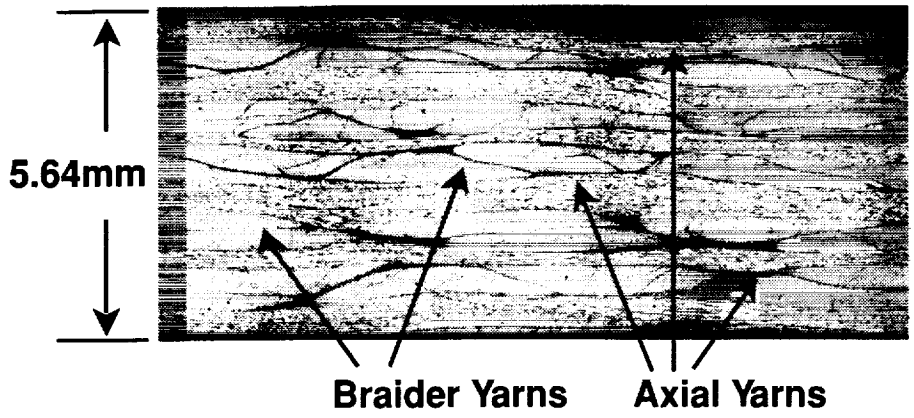

(a) Longitudinal section along axial yarns

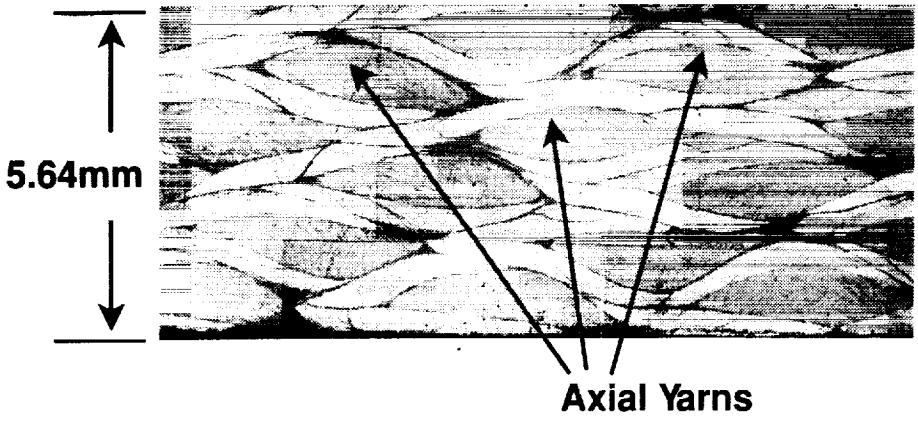

(b) Transverse section

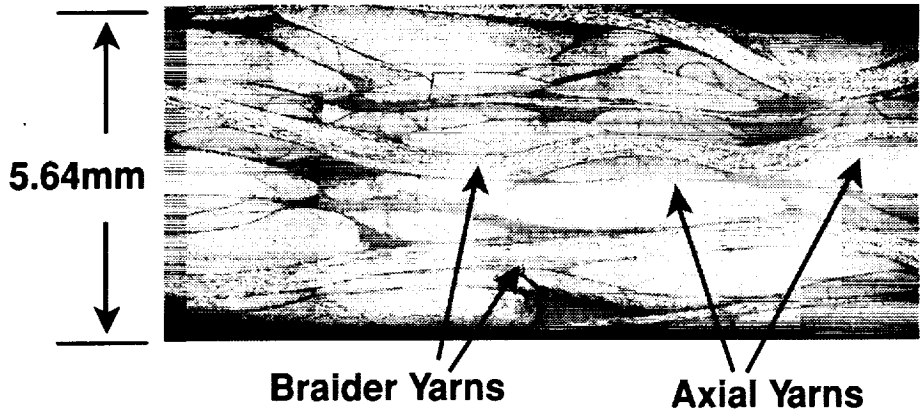

(c) Section along braider yarns

Fig. 3 - Typical cross-sectional micrographs of a 2x2, 2-D triaxial braided composite.

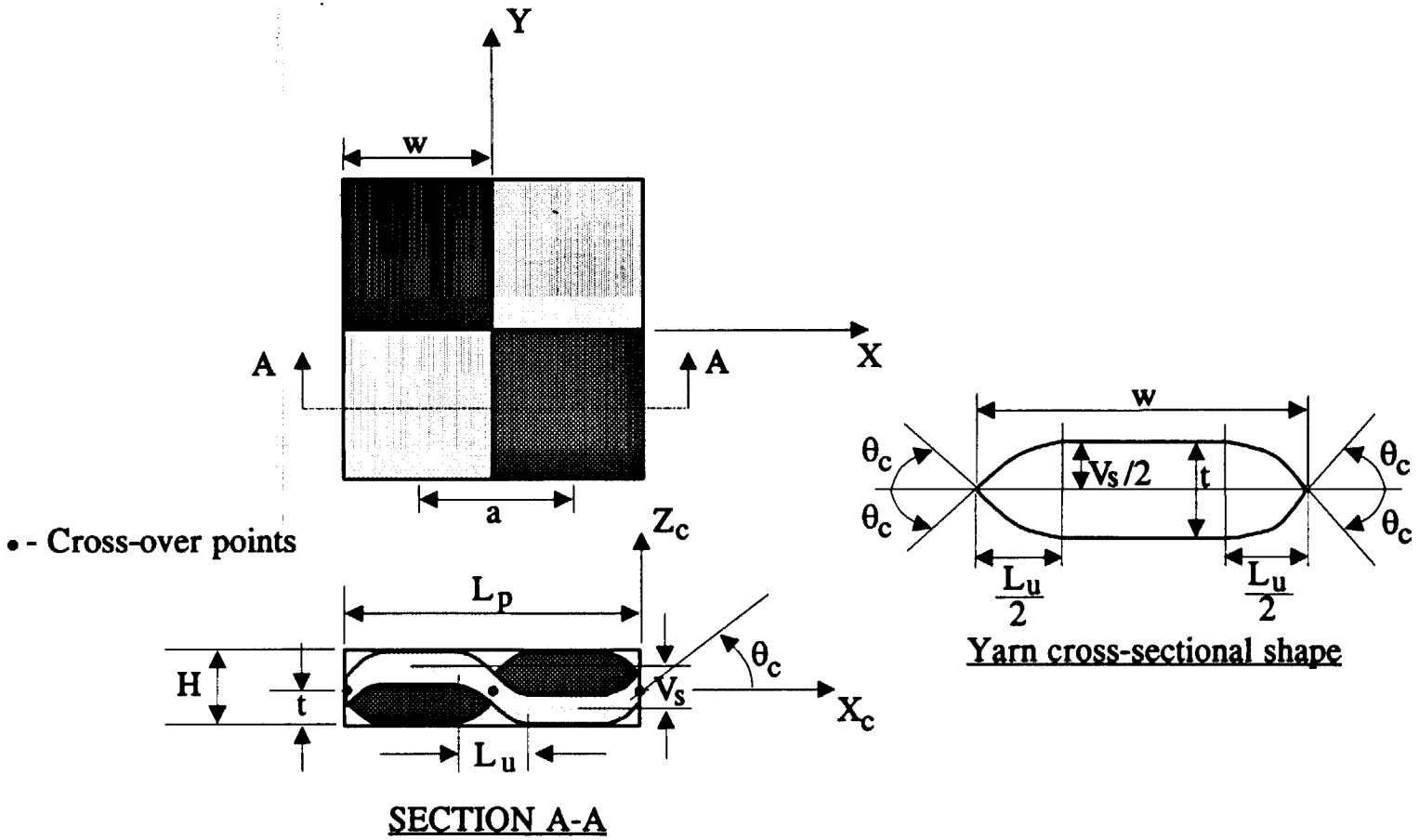

Fig. 4.- The RUC geometry and notation for a 2-D plain weave composite.

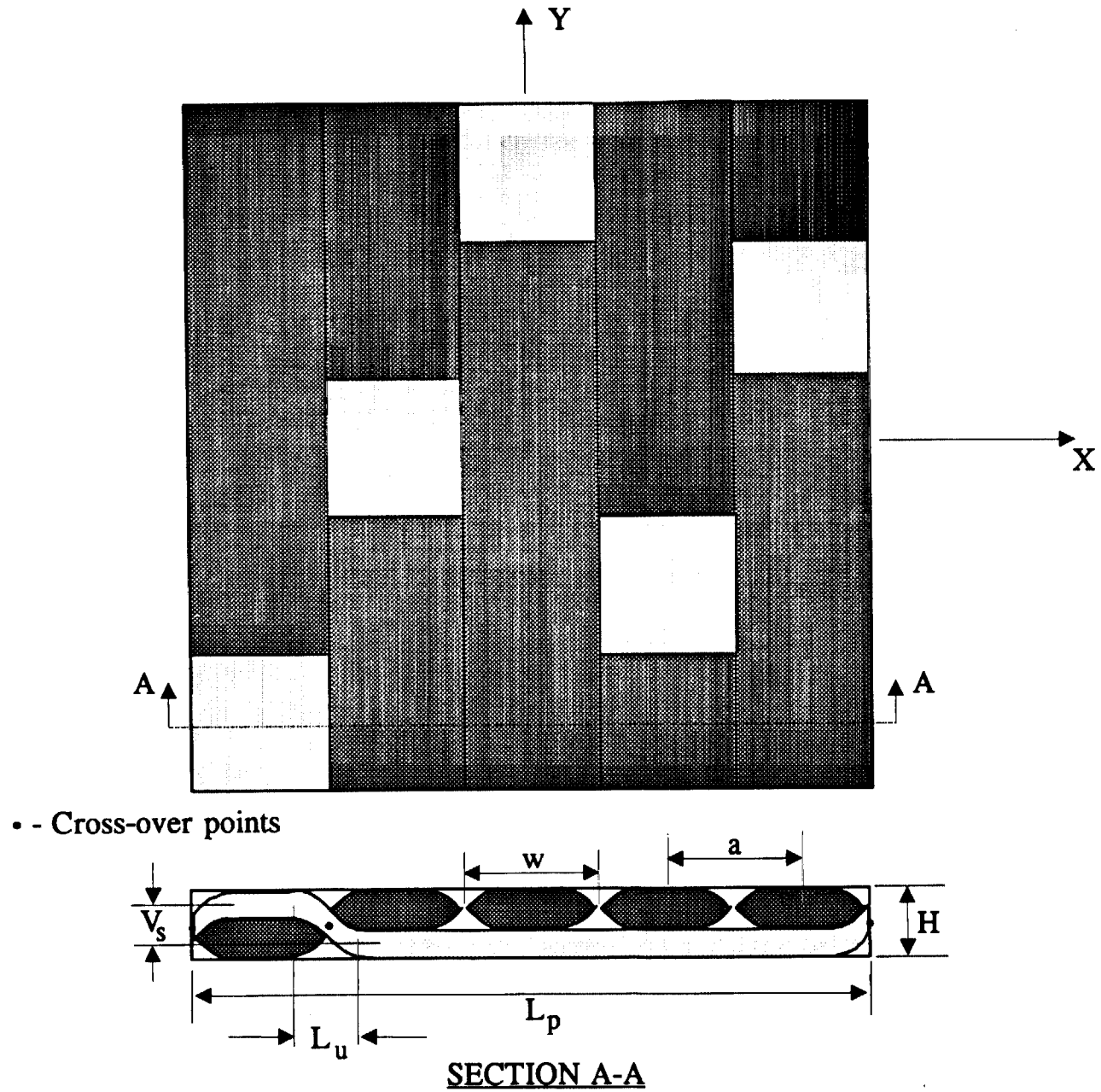

Fig. 5.- The RUC geometry and notation for a 5-harness satin weave composite.

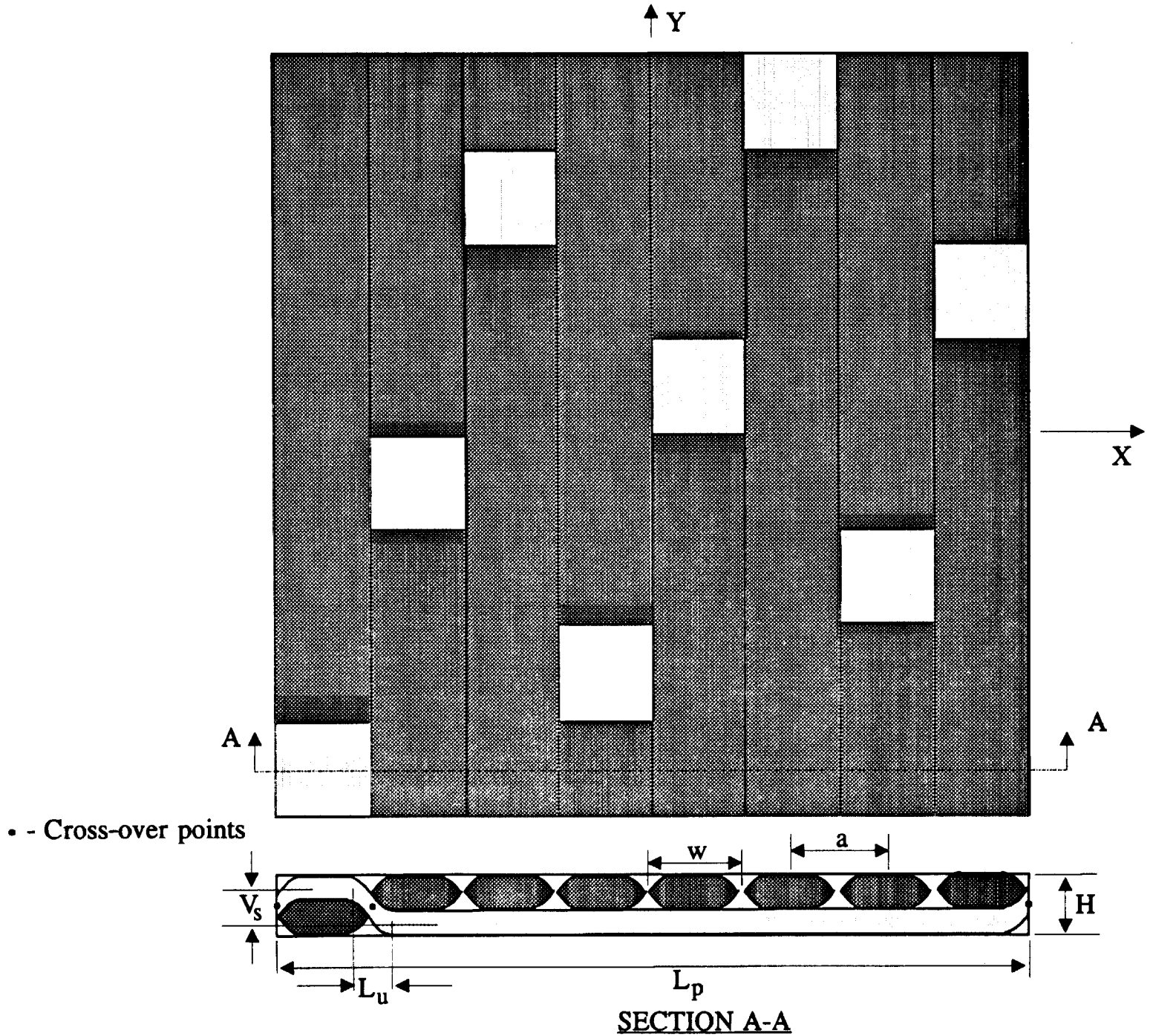

Fig. 6.- The RUC geometry and notation for an 8-harness satin weave composite.

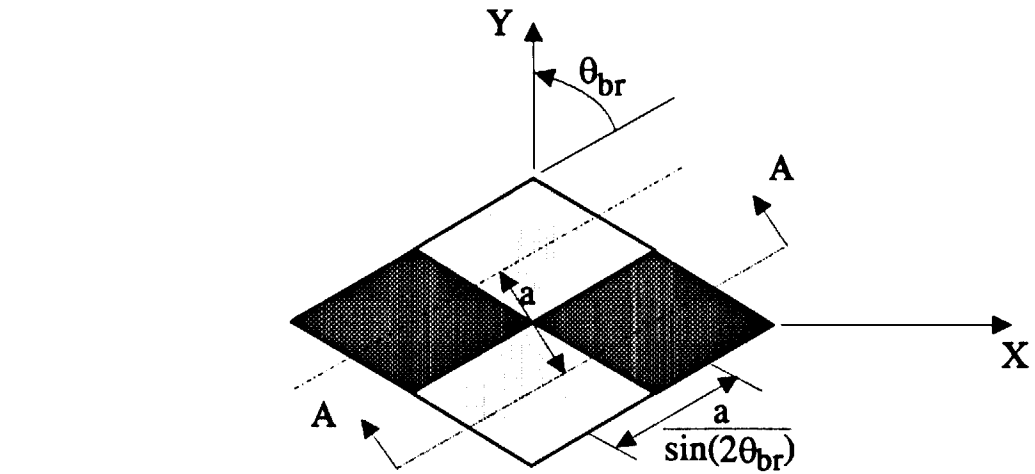

• - Cross-over points

a - perpendicular distance between yarns

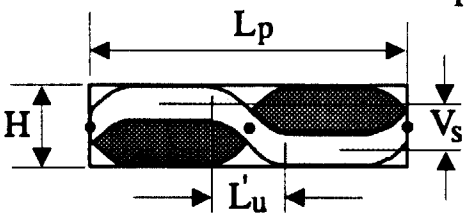

$$L'_u = \frac{L_u}{\sin(2\theta_{br})}$$

SECTION A-A

Fig. 7.- The RUC geometry and notation for a 2-D braided composite.

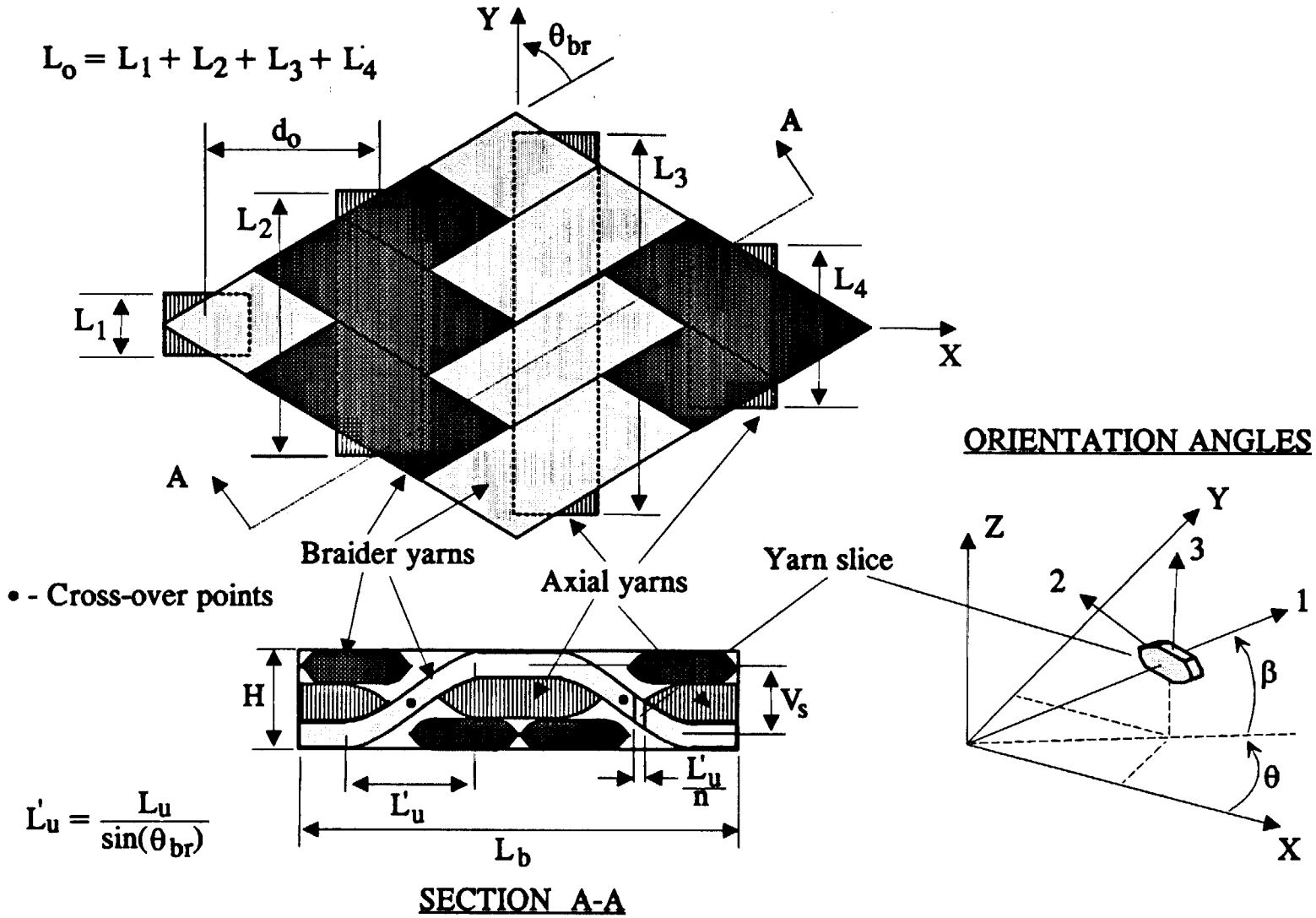

Fig. 8.- The RUC geometry and notation for a 2x2 2-D triaxial braided composite.

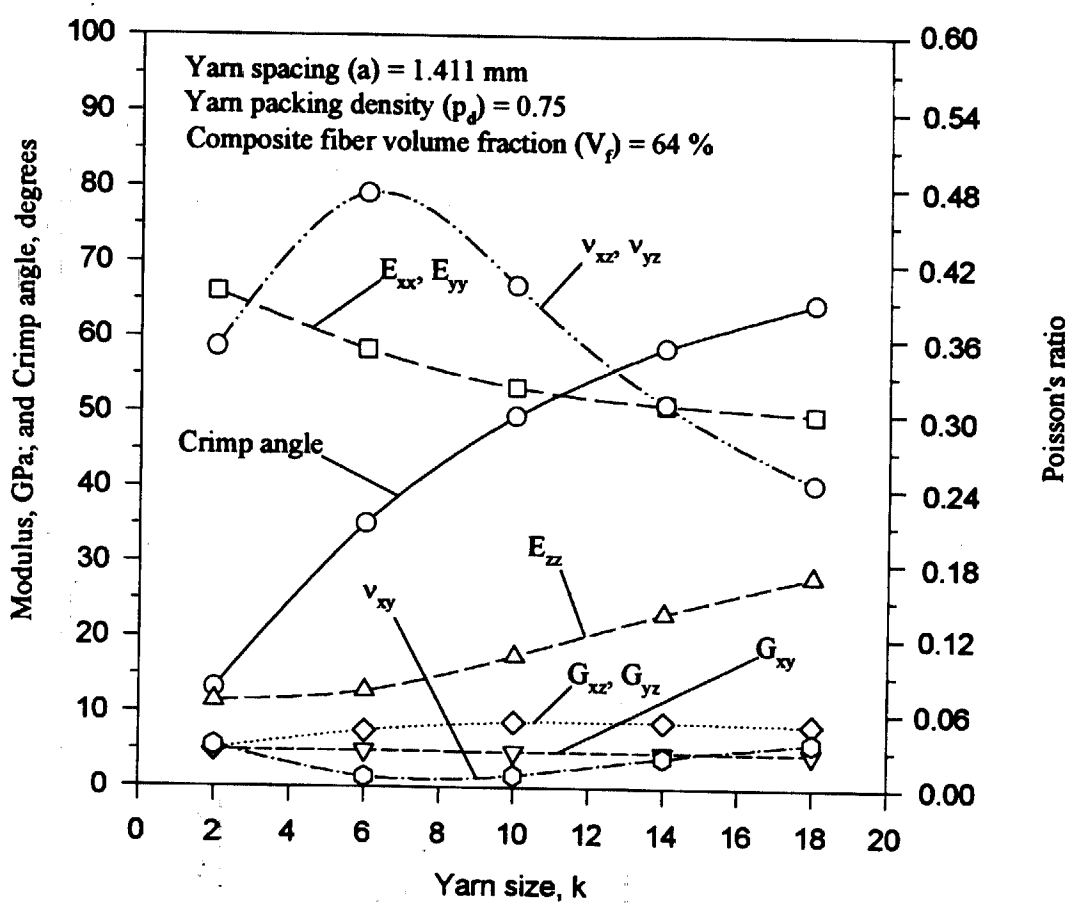

Fig. 9.- Variation of plain weave crimp angle, moduli and Poisson's ratios with yarn size.

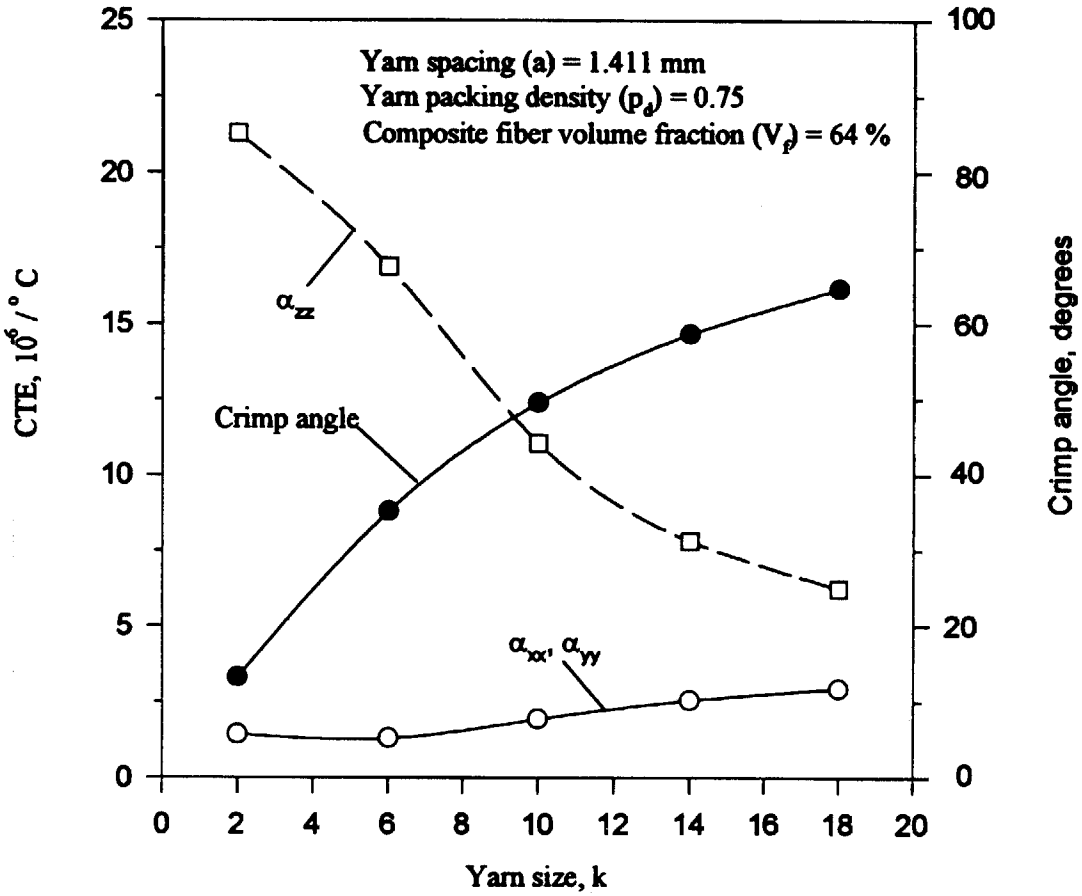

Fig. 10.- Variation of plain weave crimp angle and CTE's with yarn size.

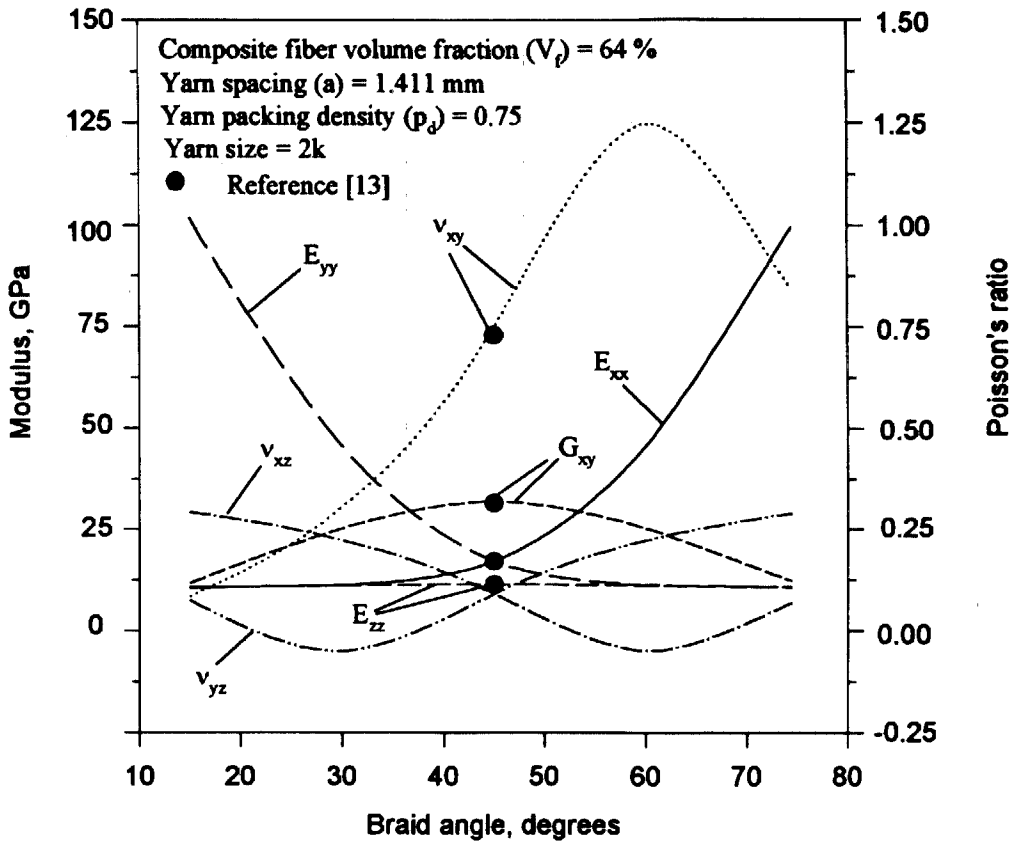

Fig. 11.- Variation of 2-D braided composite stiffnesses and Poisson's ratios with braid angle.

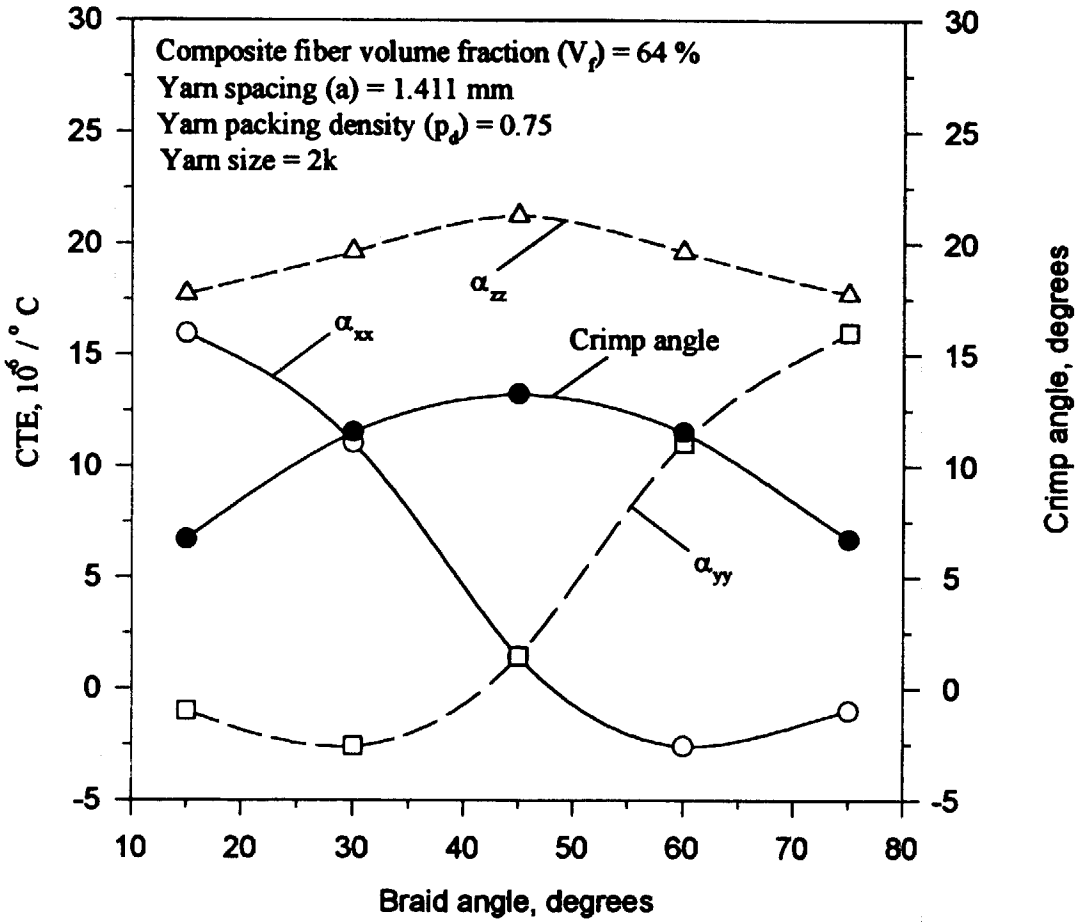

Fig. 12.- Variation of 2-D braided composite crimp angle and CTE's with braid angle.

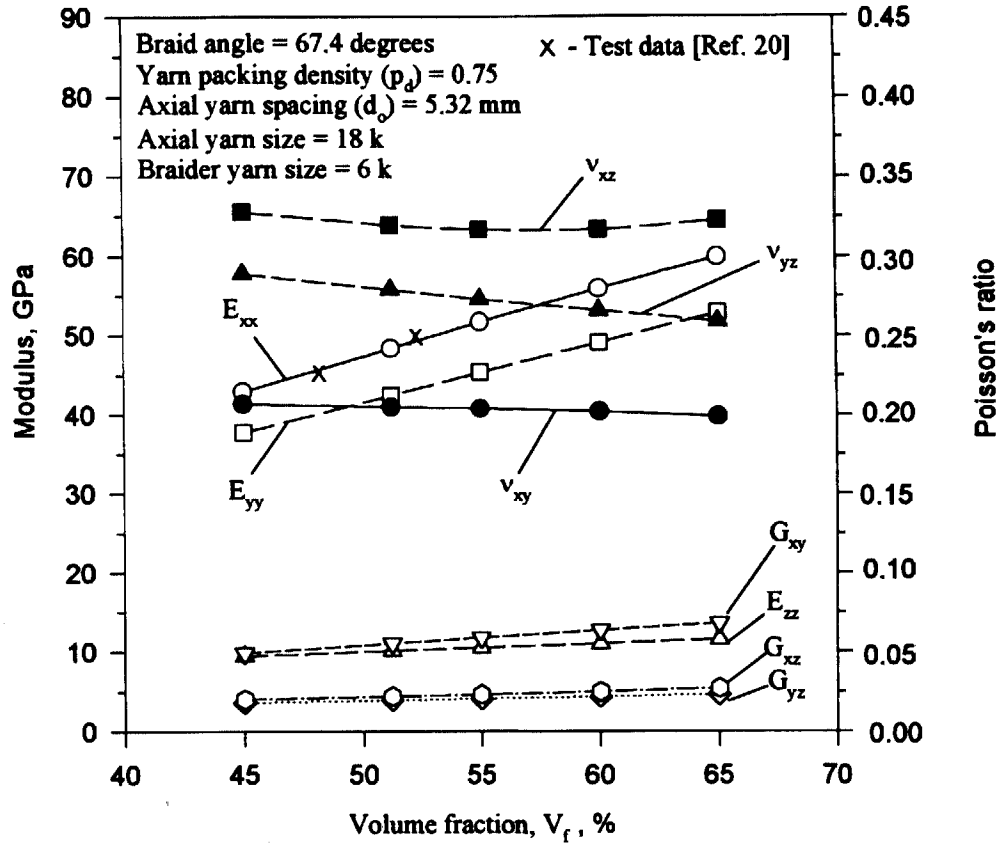

Fig. 13.- Variation of stiffnesses and Poisson's ratios with V_f for 2-D triaxial braided composite.

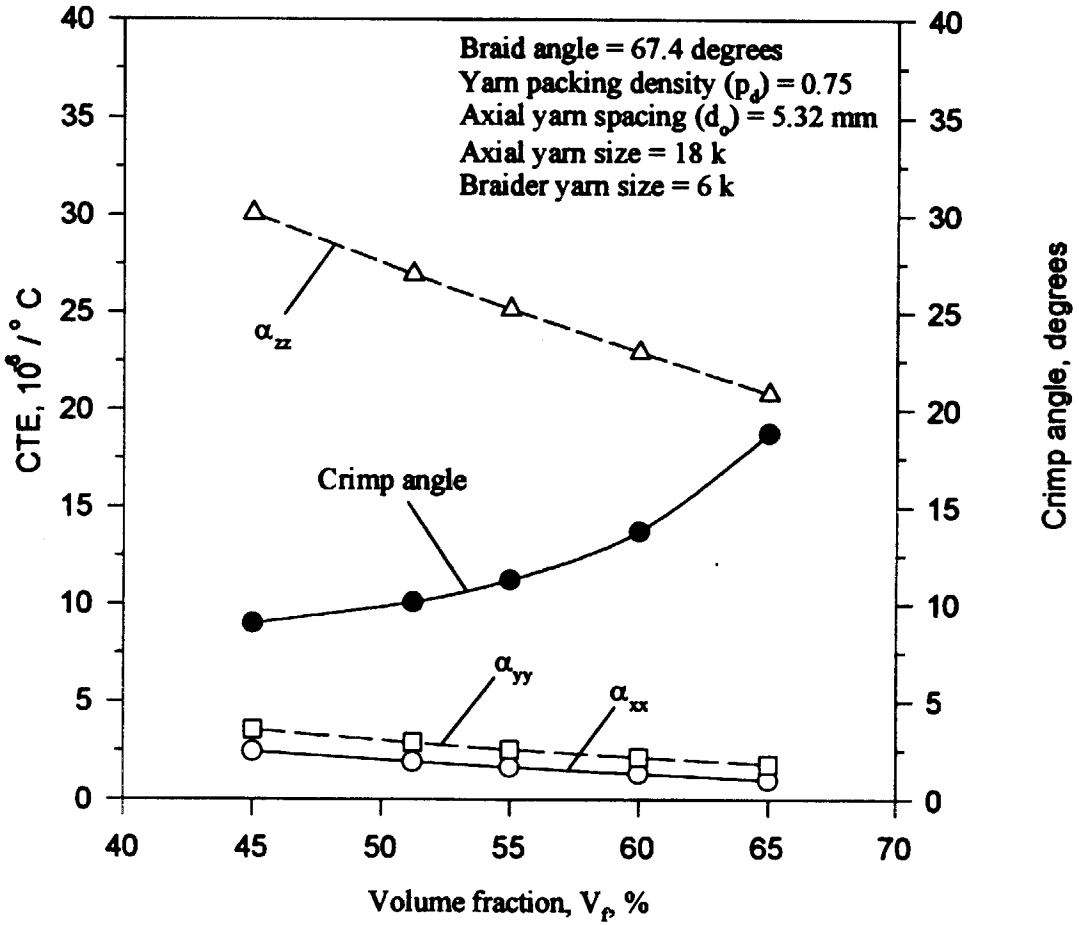

Fig. 14.- Variation of crimp angle and CTE's with V_f for 2-D triaxial braided composite.

REPORT DOCUMENTATION PAGE

Form Approved
OMB No. 0704-0188

1. AGENCY USE ONLY *(Leave blank)*	2. REPORT DATE	3. REPORT TYPE AND DATES COVERED
	June 1994	Contractor Report

4. TITLE AND SUBTITLE
Analysis of Woven and Braided Fabric Reinforced Composites

5. FUNDING NUMBERS
NAS1-19399

WU 510-02-12-09

6. AUTHOR(S)
Rajiv A. Naik

7. PERFORMING ORGANIZATION NAME(S) AND ADDRESS(ES)
Analytical Services & Materials, Inc.
Hampton, VA 23666

8. PERFORMING ORGANIZATION REPORT NUMBER

9. SPONSORING / MONITORING AGENCY NAME(S) AND ADDRESS(ES)
National Aeronautics and Space Administration
Langley Research Center
Hampton, VA 23681-0001

10. SPONSORING / MONITORING AGENCY REPORT NUMBER
NASA CR-194930

11. SUPPLEMENTARY NOTES
Langley Technical Monitor: Charles E. Harris
Presented at the ASTM 12th Symposium on Composite Materials: Testing and Design, Montreal, Canada, May 16-17, 1994.

12a. DISTRIBUTION / AVAILABILITY STATEMENT
Unclassified - Unlimited

Subject Category - 24

12b. DISTRIBUTION CODE

13. ABSTRACT *(Maximum 200 words)*

A general purpose micromechanics analysis that discretely models the yarn architecture within the textile repeating unit cell, was developed to predict overall, three dimensional, thermal and mechanical properties. This analytical technique was implemented in a user-friendly, personal computer-based, windows compatible code called Textile Composite Analysis for Design (TEXCAD). TEXCAD was used to analyze plain, 5-harness satin, and 8-harness satin weave composites along with 2-D braided and 2x2, 2-D triaxial braided composites. The calculated overall stiffnesses correlated well with available 3-D finite element results and test data for both the woven and the braided composites. Parametric studies were performed to investigate the effects of yarn size on the yarn crimp and the overall thermal and mechanical constants for plain weave composites. The effects of braid angle were investigated for the 2-D braided composites. Finally, the effects of fiber volume fraction on the yarn undulations and the thermal and mechanical properties of 2x2, 2-D triaxial braided composites were also investigated.

14. SUBJECT TERMS	15. NUMBER OF PAGES
Textile composites; Modeling; Plain weave; Satin weave; Triaxial braid; Yarn; Crimp; Design; Thermal; Stiffness; Elastic properties	46
	16. PRICE CODE: A03

17. SECURITY CLASSIFICATION OF REPORT	18. SECURITY CLASSIFICATION OF THIS PAGE	19. SECURITY CLASSIFICATION OF ABSTRACT	20. LIMITATION OF ABSTRACT
Unclassified	Unclassified		